Physics – Uspekhi **63** (4) 365 – 387 (2020)

INSTRUMENTS AND METHODS OF INVESTIGATION PACS numbers: 52.35.Hr, 52.35.Mw, 52.35.Qz

Low-power-threshold parametric decay instabilities of powerful microwave beams in toroidal fusion devices

E Z Gusakov, A Yu Popov

DOI: https://doi.org/10.3367/UFNe.2019.05.038572

Contents

Abstract. **We discuss the experimental conditions responsible for a drastic decrease in the power threshold of parametric decay instabilities under auxiliary electron cyclotron resonance heating (ECRH) in toroidal magnetic fusion devices when the upper hybrid (UH) resonance for the pump wave is absent. We show that for a finite-width pump in the presence of a nonmonotonic (hollow) density profile occurring due to plasma equilibrium in the magnetic islands or anomalous particle fluxes from the ECR layer, 3D localization of one or both daughter waves is possible. This localization leads to the full suppression of daughter wave energy losses from the decay layer and a substantial increase in the nonlinear pumping efficiency. This decreases the power threshold of nonlinear excitation, which can be easily overcome in current ECRH experiments utilizing 1 MW microwave beams. Different scenarios of extraordinary and ordinary wave decays are investigated. The secondary decays of primary daughter waves and pump wave depletion are considered as the most effective mechanisms leading to the transition of primary instability to the saturation regime. The proposed theoretical model was shown to be able to describe the anomalous phenomena discovered in ECRH experiments in different toroidal fusion devices all over the world.**

Keywords: three-wave coupling, parametric decay, microwaves, auxiliary plasma heating, toroidal devices, thermonuclear fusion

E Z Gusakov, A Yu Popov
Ioffe Institute, ul. Politekhnicheskaya 26, 194021 St. Petersburg, Russian Federation
E-mail: evgeniy.gusakov@mail.ioffe.ru, a.popov@mail.ioffe.ru

Received 21 February 2019, revised 22 April 2019
Uspekhi Fizicheskikh Nauk **190** (4) 396 – 420 (2020)
Translated by M Zh Shmatikov; edited by A M Semikhatov

1. Introduction

1.1 Parametric decay instabilities of inhomogeneous plasma

Powerful microwave beams are currently widely used both in ionospheric experiments and in controlled thermonuclear fusion facilities with magnetic confinement. At the microwave energy flow densities achieved in these experiments, the plasma behaves like a nonlinear electrodynamic medium. This behavior, in particular, manifests itself in parametric excitation of plasma eigenmodes, whose frequencies and wavevectors are related by the decay resonance condition when the pump wave field exceeds a certain threshold. The factors that most strongly stabilize the development of parametric decay instabilities are the spatial inhomogeneity of the plasma and the finite size of the interaction region in the presence of a microwave beam.

We discuss the instability of coupled modes in an inhomogeneous infinite plasma in more detail. We consider the parametric decay of a pump wave with a frequency ω_0 and a wavenumber $k_{0x}(\omega_0, x)$, which propagates along the direction of inhomogeneity x, into two daughter waves that also propagate along the direction of inhomogeneity. The so-called reduced equations for coupled mode amplitudes, which describe their nonlinear interaction with the effect of weak inhomogeneity taken into account, can be easily derived within the Wentzel–Kramers–Brillouin (WKB) approximation [1–4]:

$$\begin{aligned} &\frac{\partial a_1}{\partial t} + u_1 \frac{\partial a_1}{\partial x} + \nu_d a_1 = \nu_0 \exp\left(-\mathrm{i}\int^x \Delta K(x')\,\mathrm{d}x'\right) a_2\,, \\ &\frac{\partial a_2}{\partial t} + u_2 \frac{\partial a_2}{\partial x} + \nu_d a_2 = \nu_0^* \exp\left(\mathrm{i}\int^x \Delta K(x')\,\mathrm{d}x'\right) a_1\,, \end{aligned} \tag{1}$$

where $\Delta K(x) = k_{0x}(x) - q_{1x}(x) - q_{2x}(x)$ is the mismatch of decay resonance conditions, q_{1x} and q_{2x} are the projections of the wavevectors of the excited waves on the direction of inhomogeneity, ω_1 and $\omega_2 = \omega_0 - \omega_1$ are the frequencies of the daughter waves, u_1 and u_2 are the daughter wave group velocities in the direction of inhomogeneity x, v_d is the linear amplification coefficient, and v_0 is the coefficient, proportional to the pump wave amplitude, that describes nonlinear amplification and whose absolute value coincides with the maximum growth rate of the decay instability in the theory of homogeneous plasma. It was assumed in deriving Eqns (1) that the plane pump wave propagates along the direction of inhomogeneity x.

If the decay resonance condition mismatch is a linear function of the coordinate, parametric decay is only possible in the vicinity of the point x_d where the conditions of space synchronism or a three-wave resonance are satisfied, i.e., $\Delta K(x_d) = 0$. Solutions of system (1) can then be expressed in terms of parabolic cylinder functions. These solutions describe spatial amplification of the daughter waves, i.e., a change in their amplitudes as they pass through the resonant layer. This process can be described using the amplification matrix elements that relate the amplitudes of the waves incident on the resonant layer and escaping from it:

$$a_{1,2}^{\text{out}} = S_{11,22} a_{1,2}^{\text{in}}\,, \qquad a_{1,2}^{\text{out}} = S_{12,21} a_{2,1}^{\text{in}}\,, \tag{2}$$

$$S_{11,22} = \exp(\pi Z)\,, \qquad S_{21,12} = \pm\sqrt{\pm 2\mathrm{i}\pi}\,\frac{v_0 l_d}{|u_{2,1}|_{x_d}}\,\frac{\exp(\pi Z/2)}{\Gamma(1 \pm \mathrm{i}Z)}\,, \tag{3}$$

where $\Gamma(\ldots)$ is the Euler gamma function, $Z = |v_0|^2 l_d^2/(|u_1||u_2|)$, and $l_d = |\partial\Delta K(x_d)/\partial x|^{-1/2}$ is the size of the resonance layer. Amplification matrix (3) was obtained in [1–4] by ignoring changes in the pump wave amplitude that result from nonlinear interaction. The pump wave depletion effect was later taken into account in [5, 6], where the amplification matrix was obtained using the methods of inverse scattering theory [7]. However, in describing the initial (linear in the daughter wave amplitudes) stage of the development of the nonlinear process, pump wave depletion does not play a significant role. The amplification matrix is described by formulas (3) sufficiently well in this case.

An analysis of Eqns (2) and (3) shows that the loss of the daughter wave energy in the interaction region fully suppresses the instability if the characteristic size of the resonance region is significantly less than the characteristic amplification length. The condition is satisfied if the inequality $Z \ll 1$ holds. In the case of the inverse inequality, $Z > 1$, parametric excitation of plasma oscillations occurs in a resonant layer of a finite size l_d. However, the exponential increase in their amplitudes $a(t)$ with time is already saturated in the linear approximation, within system (1), at the level $a(+\infty) \propto a(0)\exp(\pi Z)$ [1]. From a mathematical standpoint, this is a consequence of the absence of poles in the dependence of the amplification matrix elements on the excited wave frequencies. Strictly speaking, the plasma is not unstable in this case, and decay interaction reduces to spatial amplification of a wide frequency spectrum of noise in the region of three-wave resonance, often referred to as convective. The parametric processes evolve in this case relatively sluggishly, and the excited waves are not coherent.

According to theoretical concepts of an inhomogeneous plasma, an absolute parametric decay instability can also be excited, which is saturated due to higher-order nonlinear effects. Such instability is usually excited due to spatial amplification if conditions are satisfied for at least part of the convective energy loss to be recuperated back to the decay region. The development of the theory of parametric instability of an inhomogeneous plasma made it possible to identify the conditions under which such feedback loops can emerge. The simplest option is realized if the spatial synchronism conditions are satisfied not at one but at two points and the daughter wave group velocities are oriented in opposite directions [3, 8]. The resonance decay condition mismatch is in this case a quadratic function of the coordinate, i.e., $\Delta K = \Delta K''(x^2 - x_d^2)/2$, where $\Delta K''$ is the second derivative of the resonance condition mismatch with respect to the coordinate x, and parametric decay is possible in the vicinity of the two points $x = \pm x_d$, where the spatial synchronism conditions $\Delta K(\pm x_d) = 0$ are satisfied.

If the distance between the resonance layers is much larger than the size of the coherence regions, i.e., $2|x_d| \gg |\Delta K''|_{\pm x_d}^{-1/3}$, the nonlinear amplification of daughter waves in each of the resonance layers can be considered independently. If the directions of the daughter wave group velocities are opposite, i.e., $u_1 u_2 < 0$, a feedback loop can be excited between the points $\pm x_d$ under the condition that [8]

$$S_{12} S_{21} \exp(\mathrm{i}\Phi) = \exp\left[2 x_d v_d \left(|u_1|^{-1} + |u_2|^{-1}\right)\right], \tag{4}$$

where $\Phi = \int_{-x_d}^{x_d} \Delta K(x)\,\mathrm{d}x + \pi/2$ is the phase gained by the daughter waves in the feedback loop. Condition (4) determines characteristics of the absolute parametric decay instability such as its growth rate, eigenfrequency spectrum, and power threshold. In particular, the instability power threshold is determined by the balance between amplification and losses during the propagation of waves in the feedback loop. The absolute instability growth rate is in this case of the order of the inverse time of wave energy circulation in the loop.

Another option for the emergence of a feedback loop is the excitation of daughter waves localized in one way or another in the vicinity of the parametric interaction region. The convective outflow of the excited wave energy from the decay region is not very important here because a significant part of the energy comes back due to the localization of one or both daughter waves [9, 10]. The parametric decay instability can be described in this case using a perturbative procedure [10]. At the first step, we can disregard the attenuation of daughter waves and their nonlinear amplification, assuming these effects to be small. This enables determination of the eigenfunctions $\varphi_n(x)$ and $\varphi_m(x)$ that describe the confined oscillations. Taking the attenuation and nonlinear coupling of daughter waves in the presence of a pump wave into account at the next step of the perturbative procedure, we arrive at equations for the amplitudes a_1 and a_2 of the eigenfunctions $\varphi_n(x)$ and $\varphi_m(x)$:

$$\begin{aligned} &\frac{\partial a_1}{\partial t} + \langle v_{d1}\rangle a_1 = \langle v_0\rangle a_2\,, \\ &\frac{\partial a_2}{\partial t} + \langle v_{d2}\rangle a_2 = \langle v_0^*\rangle a_1\,, \end{aligned} \tag{5}$$

where $\langle v_0\rangle$ and $\langle v_{d1,2}\rangle$ are the coefficients averaged over the region in which the confined daughter waves are localized,

$$\langle v_0\rangle = \int_{-\infty}^{\infty} v_0(x) \exp\left(-\mathrm{i}\int^x k_{0x}(x')\,\mathrm{d}x'\right) \varphi_n^*(x)\varphi_m(x)\,\mathrm{d}x\,,$$

$$\langle v_{d1,2}\rangle = \int_{-\infty}^{\infty} v_d(x)\left|\varphi_{n,m}(x)\right|^2 \mathrm{d}x\,.$$

System of equations (5) describes the excitation of absolute parametric decay instability with the growth rate

$$2\gamma = -\langle v_{d1}\rangle - \langle v_{d2}\rangle + \sqrt{\left(\langle v_{d1}\rangle - \langle v_{d2}\rangle\right)^2 + 4\left|\langle v_0\rangle\right|^2}. \qquad (6)$$

We note that excitation of parametric decay instability was analyzed in [1–10] under the assumption of a plane pump wave. This approximation disregards the effect of the transverse outflow of the daughter wave energy from the nonlinear interaction region on the threshold and the nature of the emerging decay instability in the realistic case of a wave beam.

The parametric decay of a spatially bounded pump (i.e., wave beam) propagating in a homogeneous plasma was studied in [11] under the assumption that the daughter waves propagate with the same velocity in opposite directions along the direction of the field distribution inhomogeneity in the wave beam, $u_1 = -u_2 = u$. System of equations (1) was analyzed that describes the interaction between coupled modes,

$$\begin{aligned} &\frac{\partial a_1}{\partial t} + u\,\frac{\partial a_1}{\partial x} + v_d a_1 = v_0(x) a_2\,, \\ &\frac{\partial a_2}{\partial t} - u\,\frac{\partial a_2}{\partial x} + v_d a_2 = v_0^*(x) a_1\,, \end{aligned} \qquad (7)$$

where $v_0(x) = v_0$ for $-d \leqslant x \leqslant d$ and $v_0(x) = 0$ otherwise. A solution of system (7) that exponentially increases with time, $a_{1,2}(x,t) \propto \exp(\gamma t)$, is continuous at $x = \pm d$, and exponentially decreases at infinity (as $x \to \pm\infty$) must satisfy the condition

$$Q_x \tan(2Q_x d) = k_x\,, \qquad (8)$$

where $Q_x = \left(|v_0|^2 - (\gamma + v_d)^2\right)^{1/2}$ and $k_x = (\gamma + v_d)/u$ are solutions of the dispersion equation within the beam, $-d \leqslant x \leqslant d$, and outside it at $x < -d$ and $x > d$. In the vicinity of the parametric instability threshold, condition (8) reduces to a simpler relation:

$$Q_x d = \frac{\pi}{4}\,, \qquad (9)$$

which enables determining the absolute instability growth rate in the form

$$2\gamma = 2\left(\sqrt{|v_0|^2 + \left(\frac{\pi u}{4d}\right)^2} - v_d\right). \qquad (10)$$

As shown in [12], absolute instability also occurs if a bounded wave beam propagates in a spatially inhomogeneous plasma across the inhomogeneity gradient.

Thus, the possibility of exciting absolute parametric instability has been demonstrated in some situations, both in the case of a spatially inhomogeneous plasma and a plane pump wave, and in the presence of wave beams. We note that in the situation of absolute instability, at least at its initial stage, only a discrete spectrum of plasma oscillations is excited, which enables regarding such an instability as a coherent wave process.

The picture of the parametric decay instability of an inhomogeneous plasma developed in pioneering studies [1–4] was confirmed in model experiments especially conducted with linear plasma devices [13–18]. Parametric phenomena observed in these experiments were unambiguously interpreted as a result of spatial parametric amplification of waves in an inhomogeneous plasma. Notably, the characteristic structure of plasma noise in the region of spatial amplification was visualized [13]. The experiments also demonstrated the excitation of absolute parametric instability of an inhomogeneous plasma that develops as a result of spatial amplification in the presence of a feedback loop due to the complex spatial structure of the pump wave [14, 15]. Also observed in [16, 17] was the excitation of the absolute parametric instability of an inhomogeneous plasma in the presence of two decay points predicted in [3]. In particular, it was shown experimentally that absolute parametric instabilities of a nonuniform plasma occur as coherent parametric phenomena [16–18], as predicted theoretically.

Based on the three-wave resonance interaction model proposed in pioneering studies [1–4], the most dangerous scenarios of parametric decays of electromagnetic waves of various frequency ranges were studied in the late 1970s and the early 1980s. In particular, various scenarios of parametric decay of a pump wave [19–32] in a laser plasma were analyzed in detail. The experimental results, which can be found in [33–35], are in reasonable agreement with theoretical dependences and predictions. In addition, wave decay thresholds have been found in the lower hybrid frequency range [36–38]. The results of this analysis are discussed in detail, with reference to publications, in reviews [39, 40]. The experimental data obtained using various toroidal installations [41, 42] confirmed the basic patterns predicted by the theory.

1.2 Parametric decay instabilities in electron cyclotron resonant plasma heating

In the mid-1970s, the use of microwaves in the electron cyclotron (EC) frequency range [43–45] for auxiliary plasma heating of toroidal installations commenced (Tuman-2, TM-3, FT-1). The first experiments on high-power electron cyclotron resonance heating (ECRH) of plasma in toroidal installations of controlled thermonuclear fusion were carried out in the early to mid-1980s using the T-10 tokamak [46–49] using efficient and relatively compact generators ('gyrotrons') developed at the Institute of Applied Physics (IAP) of the Russian Academy of Sciences. Since then, this heating method has been successfully used and is now widely employed in most toroidal installations worldwide (for example, DIII-D, ASDEX (Axially Symmetric Divertor EXperiment) Upgrade, Wendelstein-7AS, LHD (Large Helical Device), T-10, and Wendelstein-7X) [50–59]. Over the years, a large amount of physical research has been carried out on stabilizing the plasma column and suppressing its instabilities by means of local energy deposition, pre-ionization, and pre-heating of the tokamak plasma, and control of the current and electron temperature profiles.

Propagation of microwaves in an inhomogeneous high-temperature plasma has also been analyzed theoretically. In particular, the possibility of exciting nonlinear processes, such as parametric decay instabilities of a pump wave [60–62], has been studied using the model developed in [1–4]. The estimated thresholds of these nonlinear phenomena (at the level of 1 GW for the induced scattering instability and 10 MW for the parametric decay instability) seemed to make

these phenomena experimentally unobservable. An exception was ECRH experiments that used electron Bernstein (EB) waves (short-wave electrostatic oscillations whose frequency is close to the EC frequency or its harmonics), where the upper hybrid (UH) resonance for the pump wave is excited [63–66].

The accumulated experimental data confirmed the principal theoretical estimates and predictions. As a result, the following understanding of this auxiliary plasma heating method has taken shape: ECRH is technically reliable, the pump wave energy profile can be predicted with reasonable accuracy, and microwaves in plasma do not experience losses due to nonlinear decay processes during propagation. Owing to this, it was recommended to use ECRH in the newly created International Experimental Tokamak Reactor (IETR) to heat plasma and control neoclassical tearing instability.

However, over the past few years, a wealth of data has been obtained that indicate the presence of anomalous phenomena during the propagation of microwaves in the toroidal installation plasma. In particular, abnormal radiation from the plasma was recorded during ECRH in various tokamaks and stellarators in the frequency range shifted downward relative to the heating radiation frequency. The discovered effect exhibited a pronounced threshold and nonlinear character (in terms of the heating power). As a result, the recorded signal was interpreted as anomalous scattering of heating radiation [67–72]. The most impressive results were obtained in detailed measurements on a TEXTOR tokamak (Torus EXperiment for Technology Oriented Research) [67, 70]. Auxiliary electron heating in the region of a magnetic island was used in this setup to control the development of neoclassical tearing instability.

The TEXTOR Tokamak is a facility for magnetic confinement of high-temperature plasma with circular magnetic surfaces and the following characteristics: $R_0 = 1.75$ m is the major installation radius, $a = 0.46$ m is the minor radius, and $T_e = 600$ eV and $H = 2$ T are the electron temperature and magnetic field in the magnetic island region. An extraordinary-polarization pump wave at the frequency $f_0 =$ 140 GHz was launched into the plasma in the equatorial plane of the setup from the outer side of the torus (from the side of a low magnetic field). The second harmonic of the EC resonance $2\omega_c(x_{ECR}) = \omega_0$ was located on the side of a strong magnetic field, approximately at the radius $x_{ECR} = R_{ECR} - R_0 = -28$ cm in the region where a poloidally rotating magnetic island crossed the equatorial plane of the setup (Fig. 1). We note that the anomalous scattering of microwave beams was also observed in ECRH experiments at the fundamental harmonic of the EC resonance. In particular, this effect was revealed in the FTU (Frascati Tokamak Upgrade) [72] ($R_0 = 0.935$ m, $a = 0.31$ m, $T_e = 350$ eV, and $H = 4.6$ T in the decay region, with $f_0 = 140$ GHz).

In addition, the generation of fast ions was detected in ECRH experiments [73–76]. Because there are no linear mechanisms for the effective interaction between microwaves and plasma ions, this phenomenon indicated the nonlinear nature of their behavior in plasma. Thus, the experimental data proved to strongly disagree with the theoretical concepts developed in [60–62]. This disagreement, on the one hand, was an important scientific problem, solving which required a theory of nonlinear wave interactions in an inhomogeneous magnetized plasma to be developed, and, on the other hand, was an applied problem that

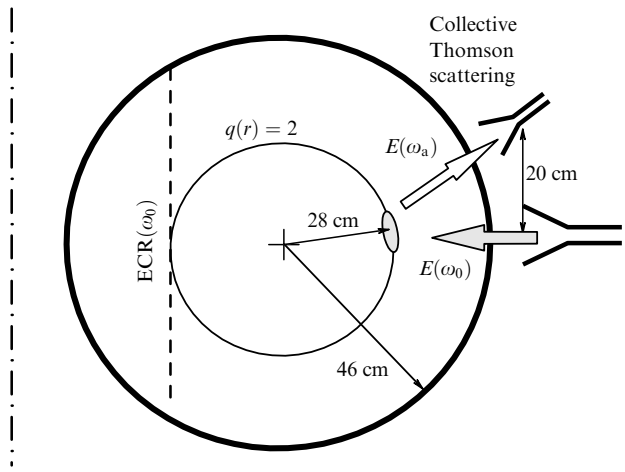

Figure 1. Schematic of an ECRH experiment using the TEXTOR tokamak [67, 70]. ECR(ω_0) is the electron cyclotron resonance at the frequency ω_0. $E(\omega_0)$ is the electric field of the pump wave at ω_0, $E(\omega_a)$ is the electric field of the plasma radiation at the frequency ω_a at which the plasma radiation is measured, $q(r) = rB_t/(R_0 B_p)$ is the safety factor, where r is the current small radius of the magnetic surface, B_t and B_p are the current values of the toroidal and poloidal magnetic fields, and $R_0 = 175$ cm is the large radius of the installation. The poloidal section of the installation is shown. A beam of extraordinary-polarization pump waves is shown in the equatorial plane of the setup, which at a radius of 28 cm crosses the magnetic island O-point (schematically represented by a shaded oval, the O-point coinciding with its center), which rotates in the poloidal direction. The second harmonic of the EC resonance for the pump wave is located on the side of a strong magnetic field. Radiation from plasma is detected by an antenna shifted from the equatorial plane by 20 cm; $a = 46$ cm is the small radius of the installation. The electron temperature in the magnetic island region is $T_e = 600$ eV and the magnetic field is $H = 2$ T.

involved assessing the possibility of correctly predicting the nature of propagation and the location where microwaves are absorbed in thermonuclear installations.

In response to the problems encountered in explaining the experimental data, efforts were made to clarify the nature of these phenomena. It was noted that all the anomalous phenomena were discovered in the discharges where the observed plasma density profile was nonmonotonic (or hollow, i.e., with a minimum at the discharge center). In particular, a nonmonotonic density profile was detected in discharges where tearing instability developed and a magnetic island was formed. The local density maximum corresponded to the magnetic island O-point. These data were obtained in the TEXTOR tokamak using a RADAR reflectometer [77] and Thomson laser scattering [78]. A nonmonotonic plasma density profile in the presence of a magnetic island was also recorded in the Tore-Supra tokamak using a sweeping reflectometer [79] and in the Tuman-3M tokamak using interferometric diagnostics [80]. A hollow density profile was observed and the mechanism of its formation was studied with a powerful central ECRH of plasma in the TCV (Tokamak à configuration variable), TJ-II [73–76], and T-10 tokamak [58]. According to the results of the analysis, such a profile is formed as a consequence of anomalous convective pump-out of plasma from the intense heating region (electron pump-out effect).

It was suggested based on the experimental data, which confirm the presence of a nonmonotonic plasma density profile, that the parametric instability thresholds are significantly reduced with such a profile [81]. This suppression can be caused by the excitation of daughter waves localized along

the direction of inhomogeneity in the vicinity of a local maximum of the density profile. Then the convective energy losses in the nonlinear interaction region turn out to be completely suppressed, which ensures intense nonlinear amplification of these oscillations.

Several scenarios of low-threshold decay of an extraordinary pump wave have been considered. The first of these is the reflective parametric decay instability of induced scattering. As this instability develops, the pump wave excites the ion Bernstein (IB) wave confined in the direction of inhomogeneity, which is a short-wavelength electrostatic oscillation with a frequency close to the ion cyclotron (IC) frequency or its harmonics, and a fast extraordinary wave at a frequency lower than that of the pump wave by the IB wave frequency. The extraordinary daughter wave propagates in the direction opposite to that of the pump wave [81–84]. The second scenario is the parametric decay [85–87], which results in the generation of an EB wave confined in the direction of inhomogeneity and an IB wave, which can leave the nonlinear interaction region, propagating in the direction toward the nearest harmonic of IC resonance. Confined along the direction of inhomogeneity, the slow IB and EB waves are also localized in the poloidal direction due to the specific inhomogeneity of the toroidal magnetic field excited by external coils [81, 83, 85].

Although beam dimensions in the toroidal direction are usually much larger than the resonance region size in the direction of inhomogeneity, both 2D confined daughter waves undergo significant energy losses in the toroidal direction from the decay region that coincides with the microwave beam 'spot' on the magnetic surface. However, it was shown in [84, 85] that due to the toroidal symmetry of the setups, the daughter wave, which is 2D localized in radius and poloidal angle, returns to the decay region along the outer circumference of the torus, which can be interpreted as the excitation of a 3D resonator for both the daughter IB wave and the daughter EB wave in both decay scenarios. The absolute instability can be excited in this case at a microwave beam power that is several orders of magnitude lower than that predicted in [60–62]. However, the growth rate of these instabilities is small, because it is proportional to the ratio of the transverse size of the microwave beam (i.e., the nonlinear interaction region) to the major radius. Due to this factor, the indicated nonlinear processes do not play a significant role in the anomalous reflection or absorption of the pump wave power.

The scenario of two-plasmon decay of an extraordinary wave into two UH waves (mainly electrostatic oscillations in the vicinity of a UH resonance) was later analyzed in [88, 89]. It was shown as a result that in the case under consideration, both daughter UH waves can be trapped in the decay region both in the direction of inhomogeneity, due to the nonmonotonic plasma density profile, and within the microwave beam. Such 3D localization enables effective nonlinear amplification of both daughter waves. The excitation threshold of this instability (up to 100 kW) is significantly lower than that predicted in [60–62] (5–6 MW). The growth rate (up to 10^8 s^{-1}) indicates the exceptional danger of such instability and the possibility of strong amplification of UH wave noise from the thermal level.

An analysis of various saturation mechanisms of the primary decay [90–93] revealed the main mechanism responsible for the relaxation of the nonlinear system to a quasi-stationary state: the secondary parametric decay instability of daughter waves, which leads to the excitation of secondary (tertiary, etc.) UH waves confined in plasma and IB waves. The cascade of secondary decays can continue as long as the generated high-frequency wave remains confined in the vicinity of the local maximum of the plasma density. As shown in Refs [60–62], the threshold of parametric instability excitation whose development generates nonlocalized UH waves cannot be exceeded for currently available generators (gyrotrons) even if they are combined into a group. This prevents subsequent decays in a natural way. The nonlinear merging of various daughter UH waves can further lead to the generation of radiation in the frequency range shifted downward relative to the pump wave frequency [93].

The proposed model made it possible to accurately reproduce both the spectrum and the radiative temperature of the electromagnetic radiation measured in experiments, in particular, using the TEXTOR tokamak [67, 70]. Moreover, this model predicts a high level of abnormal absorption of the pump wave (up to 25% power) by daughter UH and IB waves. We note that the low-frequency daughter IB waves generated during secondary instability can effectively interact with ions, leading to the generation of accelerated particle groups observed in experiments [73–76]. The frequency of nonlinearly excited UH waves significantly differs from that of the pump wave, and these waves are absorbed by the electrons at locations essentially different from those predicted under the assumption of the linear behavior of the pump wave. The difference between the power deposition profile and that predicted in the linear approximation can be at least partially responsible for the phenomenon of nonlocal heat transfer in the electron channel observed in many ECRH experiments [58].

The model developed in Refs [88–93] has a significant limitation: it requires the presence of conditions (discharge parameters) under which both daughter waves can be simultaneously localized along the direction of inhomogeneity. However, this combination of parameters is the exception rather than the rule. In the general case, in a pump wave of extraordinary and ordinary polarization decays, only one localized daughter UH wave can be excited. The second daughter wave quickly leaves the decay region along the direction of inhomogeneity, and its localization is therefore impossible. The authors of [94–97] successfully showed that a UH wave confined in the direction of inhomogeneity can be additionally localized within the microwave beam limits. Thus, a universal scenario of low-threshold parametric decay instability becomes possible: the decay of a pump wave (with ordinary and extraordinary polarization) into two daughter waves, one of which is a 3D localized UH wave whose excitation threshold is substantially (two orders of magnitude) lower than that predicted for a monotonic plasma density profile [60–62]. An analysis of the saturation of these instabilities in [98–100], taking mechanisms such as pump wave depletion and the cascade of secondary decays of primary daughter waves into account, enabled determining the saturation level and the power anomalously absorbed by daughter waves.

Furthermore, a low-threshold decay of an extraordinary wave was analyzed in the case where a 3D localized EB wave and an IB wave that leaves the decay region in the direction of inhomogeneity is excited in the vicinity of the local maximum of the density profile and within the microwave beam [102]. This scenario, which is an alter-

native to the scenario of two-plasmon decay into two UH waves, may be relevant for installations with relatively low magnetic fields [73].

The results obtained advance theoretical ideas about a three-wave resonance interaction in 3D inhomogeneous plasma and contribute to the theory of nonlinear wave transformations; they also enable a theoretical explanation, and sometimes a detailed description, of the anomalous phenomena observed experimentally during ECRH in toroidal installations. They are also of great practical importance for predicting the energy release region of a pump wave in the ITER.

In this review, we consider the mechanisms of low-threshold nonlinear excitation of a localized UH wave(s) in detail. We show that the scenarios proposed can explain the anomalous phenomena that were observed in ECRH experiments both at the second harmonic of the EC resonance (extraordinary pump wave) and at the fundamental harmonic of the resonance (ordinary pump wave). To illustrate the obtained analytic relations, we use the parameters and experimental conditions available at the TEXTOR [67, 70] and FTU [72] tokamaks, where the most detailed measurements of the anomalous effects have been carried out and various dependences have been obtained.

2. Low-threshold decay of an extraordinary wave into two localized upper hybrid plasmons

2.1. Primary instability

In an inhomogeneous plasma in a toroidal setup, parametric decay of a microwave beam occurs in the vicinity of the point where the decay resonance conditions are satisfied. Because the characteristic dimensions of the resonance layer are much smaller than those of the inhomogeneous distributions of the temperature, density, and magnetic field, it is reasonable to use a Cartesian coordinate system (x, y, z) centered at a point that corresponds to a local maximum of the density profile, with the coordinate x oriented along the direction of inhomogeneity and z directed along the magnetic field vector $\mathbf{H} = (0, 0, H)$. The field of an extraordinary electromagnetic wave that is incident on the decay resonance layer quasi-perpendicularly to the external magnetic field and propagates into the plasma along the x axis has the following form in the WKB approximation:

$$\mathbf{E}_0(\mathbf{r}, t) = \sqrt{\frac{\omega_0}{ck_{0x}(x)}} \times \left[\frac{\mathbf{e}_0 E_\mathrm{i}}{2} \exp\left(\mathrm{i}\int^x k_{0x}(x')\,\mathrm{d}x' + \mathrm{i}k_{0z}z - \mathrm{i}\omega_0 t\right) + \mathrm{c.c.}\right], \quad (11)$$

where

$$\mathbf{e}_0 = \mathbf{e}(\omega_0, x) = -\mathrm{i}\,\frac{g_0}{\varepsilon_0}\,\mathbf{e}_x + \mathbf{e}_y \quad (12)$$

is the polarization vector, E_i is the field amplitude distribution in the beam incident on the interaction region,

$$E_\mathrm{i}(x, y, z)\Big|_{x\to-\infty} = \sqrt{\frac{8\pi}{c}\,\frac{P_0}{\pi d^2}}\,\exp\left(-\frac{y^2+z^2}{2d^2}\right), \quad (13)$$

P_0 is the beam power, d is the beam size,

$$k_{0x}(x) = \frac{\omega_0}{c}\sqrt{\frac{\varepsilon_0^2 - g_0^2}{\varepsilon_0}} \quad (14)$$

is the wavevector component along the direction of inhomogeneity, $k_{0x} \gg k_{0z}$, ε_0 and g_0 are the components of the dielectric permeability tensor transverse to the magnetic field of the 'cold' plasma at the frequency ω_0,

$$\varepsilon_0 = \varepsilon(\omega_0) = 1 - \frac{\omega_\mathrm{pe}^2}{\omega_0^2 - \omega_\mathrm{c}^2}, \qquad g_0 = g(\omega_0) = \frac{\omega_\mathrm{c}}{\omega_0}\,\frac{\omega_\mathrm{pe}^2}{\omega_0^2 - \omega_\mathrm{c}^2},$$

$\omega_\mathrm{c} = |\omega_\mathrm{ce}|$, ω_ce and ω_pe are the EC and plasma frequency, and c.c. indicates the term obtained from the first term in the right-hand side of Eqn (11) by complex conjugation.

We only consider the case where the pump wave propagation direction is strictly perpendicular to the external magnetic field, $k_{0z} = 0$, and the wave decays into daughter quasi-electrostatic UH waves whose frequencies are approximately equal to half the pump wave frequency, $\omega_1 \approx \omega_0/2$, $\omega_2 = \omega_0 - \omega_1$. This decay is described by the system of equations [99]

$$\begin{aligned} &\frac{\partial^2 E_{0y}}{\partial x^2} + k_{0x}^2(x) E_{0y} = -\mathrm{i}\,\frac{4\pi\omega_0}{c^2}\,J(\omega_0), \\ &\hat{D}(\phi_1) = 4\pi\rho_1, \qquad \hat{D}(\phi_2) = 4\pi\rho_2, \end{aligned} \quad (15)$$

where the first equation describes attenuation of the pump wave when it propagates through the parametric decay region, diffraction being disregarded, and the second and third equations describe parametric excitation of UH waves. In a weakly inhomogeneous plasma, the integral operators in the left-hand side of the two equations have the form

$$\hat{D}(\phi_{1,2}) = \int \frac{\mathrm{d}\mathbf{r}'\,\mathrm{d}\mathbf{q}}{(2\pi)^3}\,\exp\left[\mathrm{i}\mathbf{q}(\mathbf{r} - \mathbf{r}')\right] D_\mathrm{UH}\left(\omega_{1,2}, \mathbf{q}, \frac{x + x'}{2}\right)\phi_{1,2}(\mathbf{r}'). \quad (16)$$

The integral operator kernel D_UH coincides with the local expression for the longitudinal dielectric permittivity of a magnetoactive plasma [103] with a small electromagnetic additive. In the vicinity of the UH resonances of daughter waves, $\omega_\mathrm{UH} = (\omega_\mathrm{c}^2 + \omega_\mathrm{pe}^2)^{1/2}$ and, under the assumption that the Larmor radius is small but finite, the function D_UH has the form

$$D_\mathrm{UH}(\omega_{1,2}) = l_T^2 q_\perp^4 + \varepsilon q_\perp^2 + g^2\,\frac{\omega_{1,2}^2}{c^2} + \eta q_z^2, \quad (17)$$

where

$$q_\perp^2 = q_x^2 + q_y^2, \qquad l_T^2 = -\frac{3}{2}\,\frac{\omega_\mathrm{pe}^2}{\omega_{1,2}^2 - \omega_\mathrm{c}^2}\,\frac{v_\mathrm{te}^2}{\omega_{1,2}^2 - 4\omega_\mathrm{c}^2},$$

v_te is the thermal velocity of electrons, and $\eta(\omega_{1,2}) = 1 - \omega_\mathrm{pe}^2/\omega_{1,2}^2$ is the longitudinal component of the dielectric permeability tensor of the 'cold' plasma [103]. In the case of quasitransverse propagation of daughter UH waves along the direction of inhomogeneity, the nonlinear charge densities ρ_1 and ρ_2 and the current density $J(\omega_0) = j_y + \mathrm{i}(g_0/\varepsilon_0)j_x$ in the right-hand side of Eqns (15) can be represented in the WKB approximation as (see the Appendix)

$$\begin{aligned} &J(\omega_0) = \mathrm{i}\,\frac{\omega_0}{4\pi H}\,\chi_\mathrm{e}^\mathrm{nl}\phi_1\phi_2^*, \\ &\rho_1 = -\frac{1}{4\pi}\,\frac{E_{0y}^*}{H}\,\chi_\mathrm{e}^{\mathrm{nl}*}\phi_2, \qquad \rho_2 = -\frac{1}{4\pi}\,\frac{E_{0y}}{H}\,\chi_\mathrm{e}^\mathrm{nl}\phi_1, \end{aligned} \quad (18)$$

where

$$\chi_{\mathrm{e}}^{\mathrm{nl}} = q_{1x} q_{2x} \frac{k_0 c}{\omega_0} \frac{4\omega_{\mathrm{pe}}^2 \omega_{\mathrm{c}}^2 \omega_0^2}{(\omega_0^2 - \omega_{\mathrm{c}}^2)(\omega_0^2 - 4\omega_{\mathrm{c}}^2)^2} \times \left(7 + 3\,\frac{g_0}{\varepsilon_0}\,\frac{\omega_0}{\omega_{\mathrm{c}}} - \frac{4\omega_{\mathrm{c}}^2}{\omega_0^2}\right). \tag{19}$$

We regard the right-hand sides of Eqns (15) as small perturbations and use a perturbative procedure suggested in [9]. At the first stage of the procedure, we disregard the nonlinear amplification, the pump wave depletion, and the propagation of UH waves along the magnetic field and take into account that the UH resonance for daughter waves is located in the vicinity of a local maximum of the density profile. The WKB solutions for two uncoupled integral equations $\hat{D}(\phi_1) = 0$ and $\hat{D}(\phi_2) = 0$ have the form [89]

$$\begin{aligned} \phi_1 &= \frac{C_1}{2} \varphi_m(x) \exp\left(\mathrm{i} q_y y - \mathrm{i}\omega_1 t\right) + \text{c.c.}\,, \\ \phi_2 &= \frac{C_2}{2} \varphi_n(x) \exp\left(\mathrm{i} q_y y + \mathrm{i}\omega_2 t\right) + \text{c.c.}\,, \end{aligned} \tag{20}$$

where $C_{1,2} = \text{const}$,

$$\varphi_m(x) = \frac{1}{\sqrt{L_m^+(x)}} \exp\left(\mathrm{i}\int_{x_{\mathrm{l}m}^*}^{x} q_x^+(m,\xi)\,\mathrm{d}\xi - \mathrm{i}\,\frac{\pi}{4}\right) + \frac{1}{\sqrt{L_m^-(x)}} \exp\left(\mathrm{i}\int_{x_{\mathrm{l}m}^*}^{x} q_x^-(m,\xi)\,\mathrm{d}\xi + \mathrm{i}\,\frac{\pi}{4}\right) \tag{21}$$

is an eigenfunction (the mth mode), and $L_m^{\pm}(x)$ is the geometric-optic length of the wave path between two turning points $(x_{\mathrm{l}m}^*, x_{\mathrm{r}m}^*)$,

$$L_m^{\pm}(x) = D_{mq}^{\pm} \int_{x_{\mathrm{l}m}^*}^{x_{\mathrm{r}m}^*} \mathrm{d}\xi \left(\frac{1}{D_{mq}^+(\xi)} + \frac{1}{D_{mq}^-(\xi)}\right).$$

The wavevector components in the direction of inhomogeneity

$$q_x^{\pm} = \sqrt{\frac{-\varepsilon(x) \mp \sqrt{\varepsilon^2(x) - 4\omega^2 g^2(x) l_T^2/c^2}}{2 l_T^2} - q_y^2} \gg q_y \tag{22}$$

are solutions of the dispersion equation $D_{\mathrm{UH}} = 0$ at $q_z = 0$. Away from the UH resonance, they describe the 'warm' (+) and 'cold' (−) branches of the UH wave dispersion curve. The frequencies of the daughter UH waves $\omega_1 = \omega^m$ and $\omega_2 = \omega_0 - \omega^m$ and their poloidal wavenumbers $q_y^{m,n}$ satisfy the quantization conditions

$$\begin{aligned} &\int_{x_{\mathrm{l}m}^*}^{x_{\mathrm{r}m}^*} \left(q_{1x}^+(\xi) - q_{1x}^-(\xi)\right) \mathrm{d}\xi = \pi(2m+1)\,, \\ &\int_{x_{\mathrm{l}n}^*}^{x_{\mathrm{r}n}^*} \left(q_{2x}^+(\xi) - q_{2x}^-(\xi)\right) \mathrm{d}\xi = \pi(2n+1)\,. \end{aligned} \tag{23}$$

The pre-exponential factors $D_{mq}^{\pm}(x)^{-1/2}$ in (21), where $D_{mq}^{\pm} = |\partial D_{\mathrm{UH}}(\omega^m, q_{mx}^{\pm}(x))/\partial q_x|$, ensure the conservation of the energy flux of UH waves along the direction of inhomogeneity. Thus, the eigenfunctions $\varphi_m(x)$ and $\varphi_n(x)$ in (21) describe noninteracting UH waves localized in the vicinity of a local maximum of the density profile and the UH resonance surface, which propagate strictly perpendicularly to the magnetic field in opposite directions. The normalization of the potential amplitudes was chosen such that $\int_{-\infty}^{\infty} |\varphi_n(x)|^2\,\mathrm{d}x = 1$.

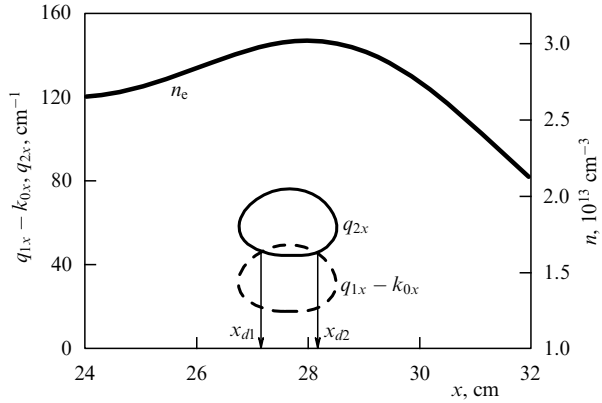

Figure 2. Dispersion curve of the first UH wave shifted downward by the pump-wave wavenumber, $q_{1x} - k_{0x}$ ($f_1^{m,n} = 70$ GHz, dashed line) and the dispersion curve of the second UH wave q_{2x} ($f_2^{m,n} = 70$ GHz, solid line) at $|q_y^{m,n}| = 0.2$ cm^{-1}, $q_z = 0$, $m = 6$, $n = 6$. The density profile n_{e} (solid bold curve) in the presence of a magnetic island [78].

Figure 2, which shows an example of the density distribution in a magnetic island (solid bold curve) [78], displays the behavior of the dispersion curves $q_{1x}^{\pm}$ and $q_{2x}^{\pm}$ of two UH waves with poloidal $q_y = 0.2$ cm^{-1} and toroidal $q_z = 0$ wavenumbers and frequencies equal to half the pump wave frequency, $f_1 = f_2 = 70$ GHz. The dashed line is the dispersion curve of the first daughter wave, which is shifted downward by the radial wavenumber of the extraordinary wave, i.e., $q_{1x} - k_{0x}$; the solid closed line is the dispersion curve of the second daughter UH wave. Both dispersion curves correspond to the oscillation eigenmode $m, n = 6$. At the points $x_{d1,2}$ where the solid and dashed curves intersect, the decay resonance conditions for the wavenumbers of the interacting waves are satisfied: $\Delta(x_{d1,2}) = k_{0x} - q_{1x} + q_{2x} = 0$. The parametric decay of the pump wave occurs in the vicinity of these points in narrow layers of the width $l_{d1,2} = |\mathrm{d}\Delta(x_{d1,2})/\mathrm{d}x|^{-1/2}$.

At the second step of the perturbative procedure, we include both the energy loss of the daughter UH waves across the direction of the plasma inhomogeneity x and their nonlinear interaction in the presence of a pump wave, whose depletion we initially ignored, assuming its amplitude to be constant. As a result, the amplitudes of the excited daughter UH waves are no longer constant: $C_{1,2} \to C_{1,2}(t, y, z)$. We substitute formula (20) in the second and third equations of system (15). We multiply both sides of the second of these equations by $\varphi_m^*(x)$, and the third by $\varphi_n^*(x)$. Next, we integrate both equations for UH waves along the x coordinate and expand the functions $\langle D_{\mathrm{UH}} \rangle$ in the neighborhood of ω^m, $q_y^{m,n}$, $q_z = 0$, where the averaging procedure $\langle \ldots \rangle$ is defined as

$$\left\langle D_{\mathrm{UH}}(\omega_{1,2}) \right\rangle = \int_{x_{\mathrm{l}m,n}^*}^{x_{\mathrm{r}m,n}^*} \mathrm{d}x \left(\frac{D_{\mathrm{UH}}\left(q_{1,2x}^+(x), x\right)}{|L_{m,n}^+(x)|} + \frac{D_{\mathrm{UH}}\left(q_{1,2x}^-(x), x\right)}{|L_{m,n}^-(x)|}\right). \tag{24}$$

As a result, we obtain a system of equations for the amplitudes of nonlinearly coupled UH oscillations [89],

$$\begin{aligned} &\frac{\partial a_1}{\partial t} + u_{my}\frac{\partial a_1}{\partial y} - \mathrm{i}\Lambda_{mz}\frac{\partial^2 a_1}{\partial z^2} = \sqrt{\frac{\omega_1}{\omega_2}}\, v_0(y,z)a_2\,, \\ &\frac{\partial a_2}{\partial t} - u_{ny}\frac{\partial a_2}{\partial y} + \mathrm{i}\Lambda_{nz}\frac{\partial^2 a_2}{\partial z^2} = \sqrt{\frac{\omega_2}{\omega_1}}\, v_0^*(y,z)a_1\,, \end{aligned} \tag{25}$$

where

$$v_0(y,z) = -\mathrm{i}\,\frac{E_{\mathrm{i}}(x,y,z)\Big|_{x\to-\infty}}{2\sqrt{\langle D_{1\omega}\rangle\langle D_{2\omega}\rangle}H} \times \int_{-\infty}^{\infty}\mathrm{d}x\,\sqrt{\frac{\omega_0}{ck_{0x}(x)}}\,\chi_{\mathrm{e}}^{\mathrm{nl}}(x)\varphi_m^*(x)\varphi_n(x)\exp\left(\mathrm{i}\int^x k_{0x}(x')\,\mathrm{d}x'\right) \tag{26}$$

is the nonlinear coupling coefficient, $D_{1,2} = D_{\mathrm{UH}}(\omega_{1,2})$, $D_{1,2\omega} = |\partial D_{1,2}/\partial\omega|$, $u_{m,ny} = \langle\partial D_{1,2}/\partial q_y\rangle/\langle D_{1,2\omega}\rangle$ are the group velocities averaged over the region of localization of plasmons, which describe convective losses (the mth and nth modes) in the poloidal direction, and $\Lambda_{m,nz} = \langle\partial^2 D_{1,2}/(2\partial q_z^2)\rangle/\langle D_{1,2\omega}\rangle$ are the coefficients, averaged over the UH plasmon localization region, of the mth and nth modes, which describe their 'diffraction' losses along the magnetic field. In Eqns (25), we normalized the daughter UH wave amplitudes as

$$a_{1,2} = C_{1,2}\sqrt{\frac{\omega_{1,2}\langle D_{1,2\omega}\rangle d^2}{16T_{\mathrm{e}}}}\,, \tag{27}$$

which means that the absolute value squared of the corresponding wave amplitude is equal to its energy density in the decay region measured in local temperature units. We note that for the decay illustrated in Fig. 2, $\omega_1 = \omega_2 = \omega^m$, $u_{my} = u_{ny} = u_y$, $\Lambda_{mz} = \Lambda_{nz} = \Lambda_z$. We focus on this particular case in what follows.

System of equations (25) describes the nonlinear coupling of UH waves in the presence of a pump wave with a constant amplitude and provides a suitable description of the early (linear) stage of parametric instability. With sufficient daughter wave amplification described by the right-hand side of Eqns (25), even weak feedback that ensures recuperation to the nonlinear interaction region of part of the energy lost by these daughter oscillations due to convection or diffraction in the decay region results in an exponential growth of the decay wave amplitudes with time. This phenomenon is equivalent to the excitation of the absolute instability of the pump wave.

In the case of convective energy loss by daughter waves in opposite directions from the nonlinear interaction region to the exterior of the one-dimensional wave beam, such absolute instability was first discovered by Kroll [104] in analyzing stimulated Mandelstam–Brillouin scattering at the laser focus; it was explored later in detail in the one-dimensional case, in particular, by Gorbunov [11]. These studies showed that for a certain transverse size of the wave beam, the energy losses of daughter waves do not compensate their growth in the strong-field region, and parametric instability can become absolute when the growing waves are captured by the strong field region of the pump wave.

Next, we generalize the results in [11, 104] to the physically realistic case of a 2D wave beam. Because the equations of system (25) are linear in the interacting wave amplitude, we seek a solution in the geometric-optic approximation $\propto \exp(\gamma t + \mathrm{i}S(y,z))$, which leads us to the equation for the eikonal:

$$\left[u_y\frac{\partial S}{\partial y} + \Lambda_z\left(\frac{\partial S}{\partial z}\right)^2\right]^2 - \left|v_0(y,z)\right|^2 + \gamma^2 = 0\,. \tag{28}$$

An analysis of partial differential equation (28) using the ray tracing method showed the presence of additional 2D localization of the UH wave trajectories on a magnetic surface within the microwave beam 'spot'. Figure 3 shows the trajectory of a daughter wave when it is nonlinearly coupled to the second daughter wave in the presence of Gaussian microwave beam (13) with the power $P_0 = 600$ kW for various ratios between the parameters $u_y d$ and Λ_z. Equation (28) can also be solved in two limit cases where the wave energy losses from the interaction region prevail in one of the directions (Fig. 3a, c). The partial differential equation can be reduced in these cases to an ordinary differential equation, and the excitation threshold and the absolute instability growth rate can be estimated.

We begin the analysis with the case where diffraction along the magnetic field prevails over other losses (Fig. 3a), and the UH wave energy loss across the magnetic field can be disregarded, and hence Eqn (28) with nonseparable variables reduces to the equation

$$\Lambda_z^2 q_z^4 - \left|v_0(z)\right|^2 + \gamma^2 = 0\,, \tag{29}$$

where $q_z = \partial S/\partial z$. Assuming that $\gamma \leqslant |v_0(0)|$, we expand $|v_0(z)|^2$ in a Taylor series: $|v_0(z)|^2 \approx |v_0(0)|^2(1 - z^2/d^2)$. Using the quantization procedure, we obtain the instability growth rate for the most dangerous fundamental mode in the form [89]

$$\gamma = \sqrt{\left|v_0(0)\right|^2 - \left(\frac{9\sqrt{\pi}}{4}\,\frac{|v_0(0)|\sqrt{\Lambda_z}}{d}\,\frac{\Gamma(3/4)}{\Gamma(1/4)}\right)^{4/3}}\,, \tag{30}$$

and the equation that determines its excitation threshold [89]

$$\left|v_0(0,P_0^{\mathrm{th}})\right| = \left(\frac{\sqrt{\pi}}{2}\,\frac{\left|v_0(0,P_0^{\mathrm{th}})\right|\sqrt{\Lambda_z}}{d}\,\frac{3\Gamma(3/4)}{\Gamma(1/4)}\right)^{2/3}. \tag{31}$$

If convective losses across the magnetic field dominate (Fig. 3c), Eqn (28) acquires the form

$$u_y^2 q_y^2 - \left|v_0(y)\right|^2 + \gamma^2 = 0\,, \tag{32}$$

where $q_y = \partial S/\partial y$. Similarly to the previous case, we assume that $\gamma \leqslant |v_0(0)|$. Therefore, $|v_0(y)|^2$ can be expanded in a Taylor series: $\left|v_0(y)\right|^2 \approx \left|v_0(0)\right|^2(1 - y^2/d^2)$. Using the quantization procedure, we obtain the instability growth rate for the most dangerous fundamental mode [89]:

$$\gamma = \sqrt{\left|v_0(0)\right|^2 - \frac{|v_0(0)|u_y}{d}} \tag{33}$$

and the equation that determines its excitation threshold [89]

$$\left|v_0(0,P_0^{\mathrm{th}})\right| = \left(\left|v_0(0,P_0^{\mathrm{th}})\right|\frac{u_y}{d}\right)^{1/2}. \tag{34}$$

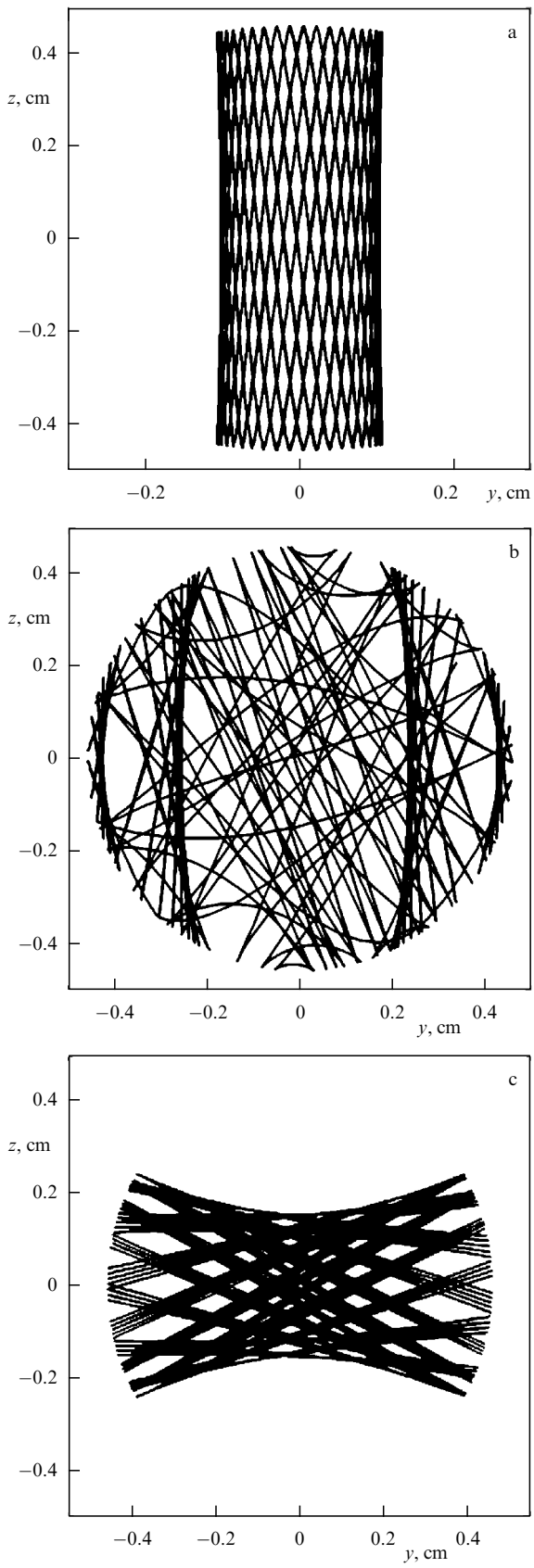

Figure 3. Trajectory of a UH wave that is a solution of Eqn (28): (a) $u_y d \ll \Lambda_z$, (b) $u_y d \approx \Lambda_z$, and (c) $u_y d \gg \Lambda_z$.

For the parameters used in the numerical solution of Eqn (28), the instability excitation threshold is $P_0^{\text{th}} = 28$ kW (Fig. 3a) and $P_0^{\text{th}} = 37$ kW (Fig. 3c).

We note that anomalous scattering of heating radiation under an auxiliary ECRH of plasma in the TEXTOR tokamak was observed whenever the magnetic island O-point passed, in the process of its poloidal rotation, through a microwave beam [67]. The plasma density profile in the nonlinear interaction region evolved in this case, which resulted in a change in the relation between the $u_y d$ and Λ_z parameters for the UH waves confined in the direction of plasma inhomogeneity. However, the UH waves remained localized in all these cases within the microwave beam (see Fig. 3). Only the instability growth rate value changed.

For the parameters we have chosen in finding the dispersion curves of the interacting waves in Fig. 2, when the island O-point crosses the microwave beam, the daughter wave energy losses from the decay region along the magnetic field dominate (Fig. 3a). The growth rate can be described in this case by analytic formula (30). Furthermore, when the island rotates, the losses along and across the magnetic field become of the same order of magnitude (Fig. 3b). It is not possible in this case to obtain an analytic expression for the instability growth rate. During further poloidal rotation, the 'potential' well parameters change such that the convective losses of the confined UH waves begin to dominate (Fig. 3c). The growth rate is given in this case by formula (33).

As a result of further rotation, the UH waves are no longer confined, and this leads to a loss of instability. Because the instability growth rate is in all cases much larger than the island rotation frequency, $1/\tau_{\text{r}} = 10^5\ \text{s}^{-1}$, but much smaller than the inverse time of the electromagnetic pump wave passage through the decay region, $1/\tau_{\text{tr}} \propto 10^{10}\ \text{s}^{-1}$, i.e., $1/\tau_{\text{r}} \ll \gamma \ll 1/\tau_{\text{tr}}$, we can, first, disregard the time evolution of the pump waves and, second, regard the change in the growth rate in the process of island rotation as an adiabatic process.

Figure 4 displays the time evolution of the instability growth rate for the microwave beam power $P_0 = 600$ kW and $d = 1$ cm. This dependence is plotted as follows. Unfilled circles correspond to formula (30), which is suitable for describing the case of dominating longitudinal losses, while the filled circles correspond to formula (33), which is suitable for the case of dominating transverse losses. The initial moment $t = 0$ corresponds to the passage of the magnetic island O-point through the beam (equatorial plane). At those moments of time when the losses in the longitudinal and transverse directions are of the same order of magnitude, the analytic formulas are, strictly speaking, inapplicable. It can be seen, however, that there is a substantial overlap between these dependences, owing to which the $\gamma(t)$ behavior can be interpolated through the entire period, until $\gamma(t) > 0$. The obtained dependence can be used to estimate the power amplification factor: $\ln S = 2\Gamma = 2\int \gamma(t)\,\mathrm{d}t \approx 0.74 \times 10^5$, a value that is too large even for amplification from the thermal level of fluctuations at the UH frequency. We can expect that the instability is saturated at a much lower level owing to nonlinear effects and, primarily, to the excitation of secondary low-threshold decay instabilities related to the generation of the UH waves confined in plasma.

2.2 Saturation of instability

We consider the saturation of the two-plasmon decay instability with a cascade of decays of daughter UH waves into secondary UH and IB waves, taking the pump wave depletion due to the initial instability into consideration. To

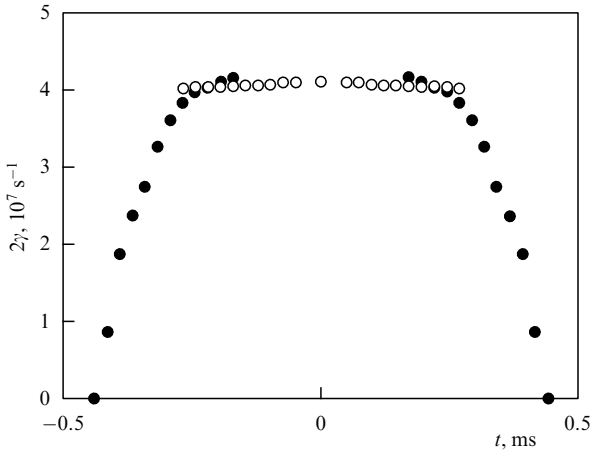

Figure 4. Time dependence of the absolute instability growth rate during the rotation of a magnetic island in ECRH experiments [67, 70].

describe the pump wave depletion, we recall that its amplitude changes as the wave passes through the resonant layer, i.e., $E_{\mathrm{i}} \to E_{\mathrm{i}}(x)$. We substitute solutions (20), (21) in the first of Eqns (15). Because the characteristic size of the nonlinear interaction region is much larger than its wavelength, but much smaller than the Rayleigh length, the equation for the $E_{\mathrm{i}}(x)$ amplitude can be obtained using the envelope method in the WKB approximation in the form [99]

$$\frac{\partial}{\partial x} E_{\mathrm{i}} = -\mathrm{i}\,\frac{\omega_0^2}{c^2}\sqrt{\frac{c}{\omega_0 k_{0x}(x)}}\,\chi_{\mathrm{e}}^{\mathrm{nl}}(x)\,\frac{\varphi_m(x)\varphi_n^*(x)}{H}\,. \tag{35}$$

We integrate Eqn (35) with boundary condition (13) to obtain the amplitude of the pump wave as it passes through the nonlinear interaction region:

$$E_{\mathrm{i}} = E_{\mathrm{i}}(x)\Big|_{x\to-\infty} - \mathrm{i}\,\frac{\omega_0^2}{c^2}\,C_1 C_2^* \int_{-\infty}^{x} \mathrm{d}x'\,\chi_{\mathrm{e}}^{\mathrm{nl}}(x')\sqrt{\frac{c}{\omega_0 k_{0x}(x')}} \times \frac{\varphi_m(x')\varphi_n^*(x')}{2H}\exp\left(-\mathrm{i}\int^{x'} k_{0x}(x'')\,\mathrm{d}x''\right), \tag{36}$$

where C_1 and C_2^* are the daughter wave amplitudes.

Next, we obtain the equations for the secondary instability of daughter waves (20). In this section, we discuss only a cascade consisting of two pump wave decays as a result of which the primary and secondary daughter waves are excited. We focus on the secondary instability with the lowest threshold: the parametric decay of primary longitudinal oscillations that results in the generation of low- and high-frequency longitudinal waves confined in the plasma [90, 91].

We begin with a description of the decay of a daughter UH wave with an amplitude ϕ_1 into secondary UH waves with an amplitude ϕ_1' and IB waves with an amplitude ϕ_{I}. This process is described by the system of equations

$$\begin{aligned} &\hat{D}(\phi_1') = 4\pi\rho_1'\,,\\ &\hat{D}(\phi_{\mathrm{I}}) = 4\pi\rho_{\mathrm{I}}\,, \end{aligned} \tag{37}$$

where the integral operators $\hat{D}(\phi_1')$ and $\hat{D}(\phi_{\mathrm{I}})$ are defined according to formula (16), but in the first equation the UH wave dispersion function (17) serves as the integral transformation kernel and in the second equation, it is the dispersion function of the longitudinal wave of the intermediate frequency range (IB wave):

$$D_{\mathrm{IB}} = q^2 + \chi_{\mathrm{e}}(\omega_{\mathrm{I}}) + \chi_{\mathrm{i}}(\omega_{\mathrm{I}})\,, \tag{38}$$

where

$$\chi_j(\omega) = \frac{2\omega_{pj}^2}{v_{\mathrm{t}j}^2}\left[1 - \frac{\omega}{|q_z|v_{\mathrm{t}j}} \times \sum_{m=-\infty}^{\infty} Z\left(\frac{\omega - m\omega_{\mathrm{c}j}}{q_z v_{\mathrm{t}j}}\right)\exp\left(-\frac{q_\perp^2 v_{\mathrm{t}j}^2}{2\omega_{\mathrm{c}j}^2}\right) I_m\left(\frac{q_\perp^2 v_{\mathrm{t}j}^2}{2\omega_{\mathrm{c}j}^2}\right)\right] \tag{39}$$

is the electron and ion susceptibilities [103], with $q_\perp^2 = q_x^2 + q_y^2$ and $j = \mathrm{e}, \mathrm{i}$.

To describe the interaction of three potential oscillations, we use the kinetic description and represent nonlinear charge densities in the form [102]

$$\begin{aligned} &\begin{pmatrix}\rho_1'\\ \rho_{\mathrm{I}}\end{pmatrix} = -\frac{|e|}{4\pi T_{\mathrm{e}}}\begin{pmatrix}\chi_{\mathrm{L}}^{\mathrm{nl}*}\phi_{\mathrm{I}}^*\phi_{\mathrm{I}}\\ \chi_{\mathrm{L}}^{\mathrm{nl}}\phi_1\phi_1'\end{pmatrix},\\ &\chi_{\mathrm{L}}^{\mathrm{nl}} = \omega_{\mathrm{pe}}^2\omega_{\mathrm{c}}\sum_{n,m}\int_0^\infty \mathrm{d}v_\perp\, f_{\mathrm{M}} \\ &\times\left(q_{1x}\,\frac{mnJ_{m+n}'(q_{1x}v_\perp/\omega_{\mathrm{c}})J_n(q_{1x}'v_\perp/\omega_{\mathrm{c}})J_m(q_{\mathrm{I}x}v_\perp/\omega_{\mathrm{c}})}{(\omega_{\mathrm{I}}' - m\omega_{\mathrm{c}})(\omega_1' - n\omega_{\mathrm{c}})}\right.\\ &+ q_{\mathrm{I}x}'\,\frac{n(m+n)J_{m+n}(q_{1x}v_\perp/\omega_{\mathrm{c}})J_n(q_{1x}'v_\perp/\omega_{\mathrm{c}})J_m'(q_{\mathrm{I}x}v_\perp/\omega_{\mathrm{c}})}{(\omega_1' + n\omega_{\mathrm{c}})\left[\omega_1 - (m+n)\omega_{\mathrm{c}}\right]}\\ &\left.- q_{1x}'\,\frac{m(m+n)J_{m+n}(q_{1x}v_\perp/\omega_{\mathrm{c}})J_n'(q_{1x}'v_\perp/\omega_{\mathrm{c}})J_m(q_{\mathrm{I}x}v_\perp/\omega_{\mathrm{c}})}{(\omega_{\mathrm{I}}' - m\omega_{\mathrm{c}})\left[\omega_1 - (m+n)\omega_{\mathrm{c}}\right]}\right), \end{aligned} \tag{40}$$

where J_m' is the derivative of the Bessel function with respect to its argument. A detailed derivation of $\chi_{\mathrm{L}}^{\mathrm{nl}}$ is presented in the Appendix. Similarly to the case of the primary instability, we analyze the secondary decay using a perturbative procedure [9]. At the first step, we ignore the nonlinear amplification and seek a solution of the homogeneous equations $\hat{D}(\phi_1') = 0$ and $\hat{D}(\phi_{\mathrm{I}}) = 0$ in the WKB approximation in the form

$$\begin{aligned} &\phi_1' = \frac{C_1'}{2}\,\varphi_p(x)\exp\left(\mathrm{i}q_y^{m,n}y - \mathrm{i}\omega_1' t\right) + \mathrm{c.c.}\,,\\ &\phi_{\mathrm{I}} = \frac{C_{\mathrm{I}}}{2\sqrt{D_{\mathrm{I}q}'(x)}}\exp\left(\mathrm{i}\int^x q_{\mathrm{I}x}'(x')\,\mathrm{d}x' + \mathrm{i}(\omega_1 - \omega_1')t\right) + \mathrm{c.c.}\,, \end{aligned} \tag{41}$$

where $C_1' = \mathrm{const}$ and $C_{\mathrm{I}} = \mathrm{const}$. The eigenfunction $\varphi_p(x)$ in the first of expressions (41), which is defined in accordance with formula (21), describes a UH wave localized in the direction of inhomogeneity. The eigenfrequency of this UH wave $\omega_1' = \omega^p$ satisfies a quantization condition similar to (23). The IB wave wavenumber is a solution of the local dispersion equation $D_{\mathrm{IB}}(\omega_1 - \omega_1', q_{\mathrm{I}x}) = 0$. The pre-exponential factor that contains the expression $D_{\mathrm{I}q} = |\partial D_{\mathrm{IB}}/\partial q_{\mathrm{I}x}|$ in the denominator ensures the energy flux conservation.

At the second step of the perturbative procedure, we take the effect of nonlinear interaction between UH and IB waves in the presence of a primary UH wave into account, as a result of which the amplitudes of the excited waves change. The possibility of this secondary nonlinear interaction is illustrated in Fig. 5, where the dashed line shows the dispersion curve of the secondary IB wave $q_{\mathrm{I}x}$ at the zero longitudinal component of the wavevector $q_{\mathrm{I}z}$, $f_{\mathrm{I}} = 0.52$ GHz, and the solid lines show the sum of the wavenumbers of the primary

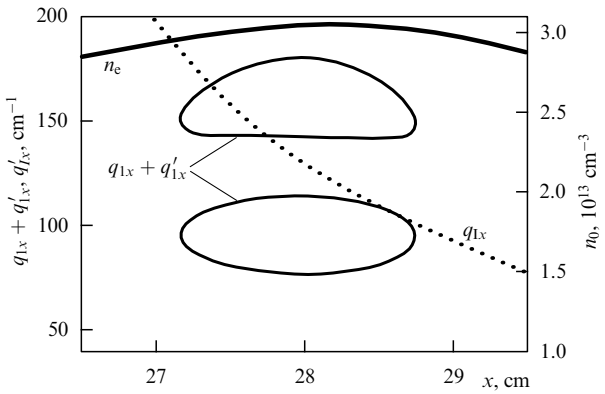

Figure 5. Dependence of the secondary IB wave wavenumber q_{1x} ($f_1 = 0.52$ GHz) (dotted curve) and the sum of the wavenumbers of the primary and secondary UH waves $q_{1x} + q'_{1x}$ ($f_1 = 70$ GHz, $f'_1 = 69.4$ GHz) (solid curves). The density profile n_e is shown with the solid bold curve.

and secondary UH waves, $q_{1x} + q'_{1x}$, $f_1 = 70$ GHz, $f'_1 = 69.47$ GHz. The decay conditions are satisfied at the points where the dispersion curves intersect, owing to which the secondary decay instability of the primary wave becomes possible in their vicinity. We also note that the daughter IB wave leaves the interaction region along the direction of inhomogeneity. For the selected parameters, the convective energy losses by the IB wave along the x axis are dominant. Because the IB wave wavevector is much larger than the inverse size of the decay layer, we can use the 'abridging' procedure to derive an equation for the envelope that describes the slow variation of the IB wave amplitude $C_I(\mathbf{r})$ from the second equation of system (41) [91]:

$$\mathrm{i}\,\frac{\partial}{\partial x}\,C_I = \frac{8\pi\rho_I}{\sqrt{D_{Iq}(x)}}\exp\left(-\mathrm{i}\int^x q_{Ix}(x')\,\mathrm{d}x' - \mathrm{i}(\omega_1 - \omega'_1)t\right).$$

We integrate this equation and substitute C_I in the right-hand side of the first equation of system (41), which we multiply by ϕ'^*_1 and integrate over x. Using a normalization similar to (27), we obtain the equation for the amplitude of the secondary UH wave localized in the radial direction [99]

$$\frac{\partial a'_1}{\partial t} + u_{py}\,\frac{\partial a'_1}{\partial y} + \mathrm{i}\Lambda_{pz}\,\frac{\partial^2 a'_1}{\partial z^2} = v_1\sqrt{\frac{\omega^p}{\omega^m}}\,|a_1|^2 a'_1\,, \tag{42}$$

where u_{py} and Λ_{pz} are the averaged group velocity and diffraction coefficient, the averaging procedure being defined in (24), and v_1 is the coefficient that describes the nonlinear interaction between the primary and secondary localized UH waves:

$$v_1 = \frac{\left|\chi_L^{\mathrm{nl}}\right|^2}{4\sqrt{\omega^p\omega^m}\,\langle D_{1\omega}\rangle\langle D'_{1\omega}\rangle}\,\frac{|e|^2}{d^2 T_e}\int_{-\infty}^{\infty}\mathrm{d}x\,\frac{\varphi_m^*(x)\varphi_p^*(x)}{\sqrt{D_{Iq}(x)}}$$
$$\times\int_x^{\infty}\mathrm{d}x'\,\frac{\varphi_m(x')\varphi_p(x')}{\sqrt{D_{Iq}(x')}}\exp\left(\mathrm{i}\int_{x'}^{x} q_{Ix}(x')\,\mathrm{d}x'\right). \tag{43}$$

We can similarly describe the secondary instability of the second primary UH wave, as a result of which secondary UH and IB waves are excited. The equation for the second secondary UH wave amplitude has the form [99]

$$\frac{\partial a'_2}{\partial t} - u_{py}\,\frac{\partial a'_2}{\partial y} - \mathrm{i}\Lambda_{pz}\,\frac{\partial^2 a'_2}{\partial z^2} = v_2\sqrt{\frac{\omega^p}{\omega^n}}\,|a_2|^2 a'_2\,, \tag{44}$$

where v_2 is defined in accordance with formula (43), $\omega_1 \to \omega_2$, $\omega'_1 \to \omega'_2$. Not only do the amplitudes of both primary waves increase as a result of primary instability. These waves also lose energy as a result of secondary decays. Given the pump wave depletion and the secondary instability of the primary daughter waves, we use system of equations (25) and Eqns (42) and (44) to derive a system of equations that describes a cascade of the decays that results in the saturation of the primary instability of the pump wave and takes the pump wave depletion into account [99]:

$$\begin{aligned}
&\frac{\partial a_1}{\partial t} + u_{my}\,\frac{\partial a_1}{\partial y} - \mathrm{i}\Lambda_{mz}\,\frac{\partial^2 a_1}{\partial z^2}\\
&\qquad = \sqrt{\frac{\omega^m}{\omega^n}}\left(v_0(y,z)a_2 - v_d|a_2|^2 a_1\right) - \sqrt{\frac{\omega^m}{\omega^p}}\,v_1|a'_1|^2 a_1\,,\\
&\frac{\partial a'_1}{\partial t} + u_{py}\,\frac{\partial a'_1}{\partial y} + \mathrm{i}\Lambda_{pz}\,\frac{\partial^2 a'_1}{\partial z^2} = \sqrt{\frac{\omega^p}{\omega^m}}\,v_1|a_1|^2 a'_1\,,\\
&\frac{\partial a_2}{\partial t} - u_{ny}\,\frac{\partial a_2}{\partial y} + \mathrm{i}\Lambda_{nz}\,\frac{\partial^2 a_2}{\partial z^2}\\
&\qquad = \sqrt{\frac{\omega^n}{\omega^m}}\left(v_0^*(y,z)a_1 - v_d|a_1|^2 a_2\right) - \sqrt{\frac{\omega^n}{\omega^p}}\,v_2|a'_2|^2 a_2\,,\\
&\frac{\partial a'_2}{\partial t} - u_{py}\,\frac{\partial a'_2}{\partial y} - \mathrm{i}\Lambda_{pz}\,\frac{\partial^2 a'_2}{\partial z^2} = \sqrt{\frac{\omega^p}{\omega^n}}\,v_2|a_2|^2 a'_2\,,
\end{aligned} \tag{45}$$

where

$$\begin{aligned}
v_d = {}&\frac{\omega_0}{\sqrt{\omega^m\omega^n}}\,\frac{4T_e}{\langle D_{1\omega}\rangle\langle D_{2\omega}\rangle c d^2 H^2}\\
&\times\int_{-\infty}^{\infty}\mathrm{d}x\sqrt{\frac{\omega_0}{ck_{0x}(x)}}\,\chi_e^{\mathrm{nl}}(x)^*\varphi_m^*(x)\varphi_n(x)\\
&\times\int_{-\infty}^{\infty}\mathrm{d}x'\sqrt{\frac{\omega_0}{ck_{0x}(x')}}\,\chi_e^{\mathrm{nl}}(x')\varphi_m(x')\varphi_n^*(x')\\
&\times\exp\left(\mathrm{i}\int_{x'}^{x} k_{0x}(x')\,\mathrm{d}x'\right)
\end{aligned} \tag{46}$$

is the coefficient that describes the pump wave depletion. The first terms in the right-hand sides of the first and third equations in (45) describe the primary instability with the pump wave depletion taken into account, while the second terms in the right-hand sides of the first and third equations and the right-hand sides of the second and fourth equations describe the secondary instability. Similar equations describing the decay cascade of a plane pump wave, i.e., $d \to \infty$, $v_0(y,z) \to v_0(0,0)$, were numerically solved in [105, 106]. The numerical solution showed that the system of nonlinear equations does not have a stationary solution in the homogeneous case. Later, it was shown numerically and analytically [107, 108] that multicomponent cnoidal waves are a solution of a system of equations similar to (45) in the homogeneous case. The primary instability is saturated as a result of switching of the interacting waves from the exponential growth mode to a strongly nonlinear oscillatory mode, in which the oscillation frequency depends on the amplitude of all the oscillations involved in the interaction. Below, we show numerically and semi-analytically that the inhomogeneity introduced into the system by the microwave beam results in the existence of a stationary solution of the system of nonlinear partial differential equations (45) with

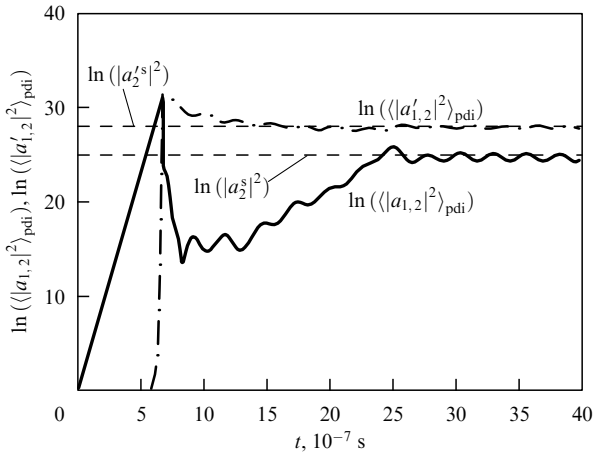

Figure 6. Evolution of the energy density of daughter primary $\langle|a_{1,2}(t)|^2\rangle_{\rm pdi}$ (solid lines, coinciding) and secondary $\langle|a_{1,2}'(t)|^2\rangle_{\rm pdi}$ (dashed-dotted lines, coinciding) plasmons in the beam 'spot.' Horizontal dashed lines indicate saturation levels (49) (bottom line) and (50) (top line).

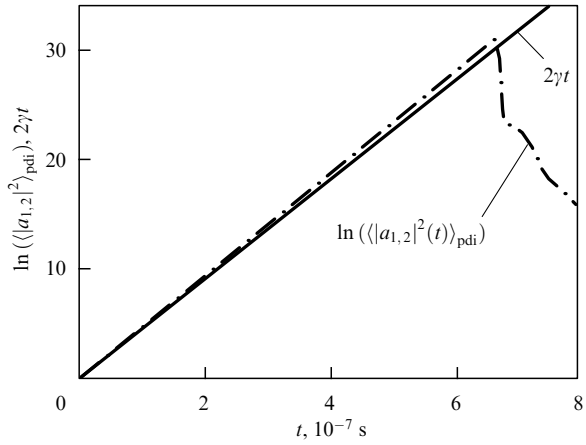

Figure 7. Amplification factor of the primary waves. The dashed-dotted lines (coinciding) show the numerical solution, and the solid line the analytic formula $2\gamma t$, where 2γ is growth rate (30).

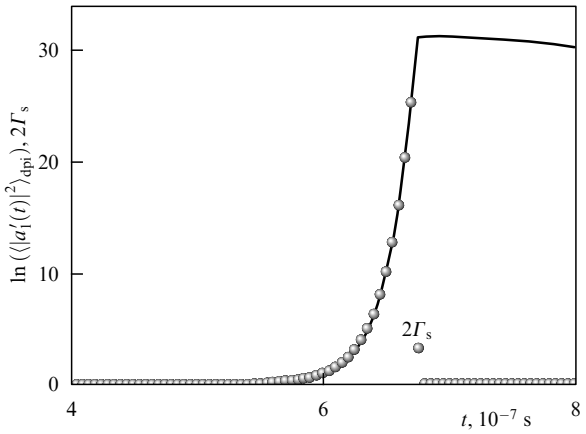

Figure 8. Amplification factor of secondary waves. The solid curve shows the numerical solution, and the dots are asymptotic expression (48).

variable coefficients, which reflects the transition of the primary instability to the saturation mode.

We now solve system of equations (45) numerically using the finite difference method in a 2D integration region $2y_{\rm B} \times 2z_{\rm B}$ whose dimensions are much larger than the microwave beam size (i.e., the nonlinear interaction region), $y_{\rm B}, z_{\rm B} \gg d$. We set periodic boundary conditions at the boundaries of this region. These conditions, which are in no way related to the toroidal geometry of the tokamak, are used to enhance the stability of the numerical scheme. Thus, the model we are considering is a simplified one and, strictly speaking, is only applicable in the vicinity of a microwave beam. It does not take into account, in particular, that the UH wave propagating inside the magnetic island approaches the EC resonance region, in which it is completely absorbed. Therefore, the breakdown of the established stationary state due to recuperation of the UH wave energy, pumped out as a result of diffraction back to the decay region, which was predicted in the model under consideration, turns out to be impossible. From a mathematical standpoint, in the model problem under consideration, we are interested only in the intermediate asymptotic behavior of the solution. In the calculation, we choose the integration region size such that the excited UH waves do not reach the boundaries in the characteristic times during which the solution reaches the intermediate saturation asymptotic behavior. In addition, we assume that the distribution of the primary and secondary daughter plasmons is homogeneous and determined by thermal fluctuations, i.e., $\langle\langle|a_{1,2}|^2\rangle\rangle = 1$, $\langle\langle|a_{1,2}'|^2\rangle\rangle = 1$, where $\langle\langle\ldots\rangle\rangle$ is statistical averaging over the ensemble of fluctuations [103]. The results of a numerical solution of system of equations (45) for a microwave beam with the power $P_0 = 600$ kW are displayed in Fig. 6, where the time dependences of the UH plasmon energy averaged over the beam (parametric decay region) are shown. The averaging procedure is defined as

$$\langle f\rangle_{\rm pdi} = \int_{-y_{\rm B}}^{y_{\rm B}}\int_{-z_{\rm B}}^{z_{\rm B}} \frac{{\rm d}y\,{\rm d}z}{\pi d^2}\, f(y,z)\exp\left(-\frac{y^2}{d^2}-\frac{z^2}{d^2}\right). \quad (47)$$

It can be seen that the energy of primary plasmons increases exponentially at the beginning. This is shown on a larger scale in Fig. 7, which shows the amplification of primary UH waves (dashed-dotted line) within the microwave beam and the analytic expression $2\gamma t$ (solid line). The primary instability growth rate 2γ is given by Eqn (30). As soon as the primary plasmon energy exceeds the secondary decay threshold, a rapid increase in the secondary UH plasmon energy can be observed (see Fig. 6). We estimate the amplification of the secondary wave:

$$2\Gamma_{\rm s}(t) = \ln\left(\left\langle\left|a_1'(t)\right|^2\right\rangle_{\rm pdi}\right) \approx \left\langle\left|a_1'(t)\right|^2\right\rangle_{\rm pdi}\frac{|\nu_1|}{|\gamma|}\,. \quad (48)$$

In Fig. 8, we compare analytic expression (48) with the numerical solution. A reasonable agreement between these dependences can be seen. The dependences in Fig. 6 show that at a certain moment the secondary plasmon energy within the pump wave 'spot' increases to the extent that it can drastically reduce the primary plasmon energy and diminish it to a level that is less than the secondary instability threshold. The secondary plasmon energy, in turn, begins to decrease, and the primary plasmon energy again increases. As a result, the system relaxes to the stationary state, and the saturation levels of corresponding plasmons can be qualitatively estimated using the following arguments. The primary plasmon energy must be such that it can compensate the losses of the secondary plasmons from the pump wave beam 'spot' and

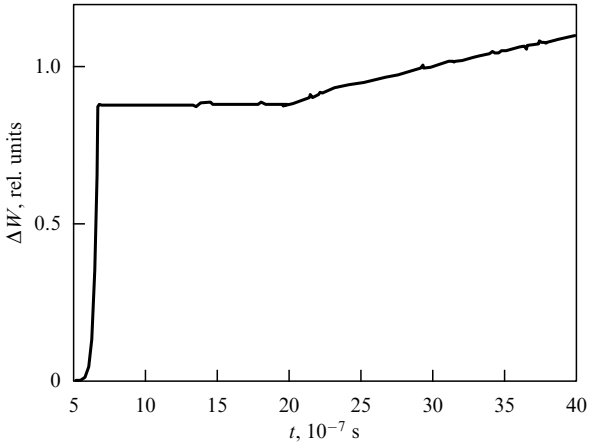

Figure 9. Evolution of the total energy of daughter plasmons in the 2D integration region $2y_B \times 2z_B$.

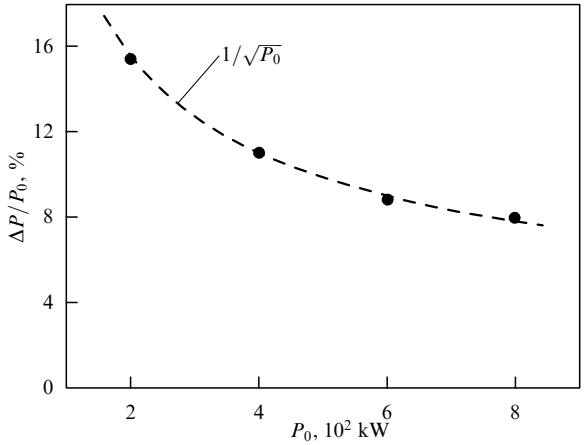

Figure 10. Fraction of the pump wave power transferred to daughter waves as a function of beam power. The dots show the result of numerical calculations (51). The dashed curve displays the dependence $\propto 1/\sqrt{P_0}$.

drive the secondary instability to virtually the excitation threshold,

$$\left|a^{\mathrm{s}}_{1,2}\right|^2 \approx \frac{1}{\tau'_{1,2}\nu_{1,2}}\,, \tag{49}$$

where $\tau'_{1,2} = \pi d^2/\Lambda_{pz}$. Therefore, the secondary plasmon energy in the saturation regime must be such that the primary instability can be kept near the excitation threshold owing to nonlinear dissipation, i.e.,

$$|a'^{\mathrm{s}}_1|^2 \simeq \frac{|\nu_0||a^{\mathrm{s}}_2|}{|\nu_1||a^{\mathrm{s}}_1|}\,, \qquad |a'^{\mathrm{s}}_2|^2 \simeq \frac{|\nu_0||a^{\mathrm{s}}_1|}{|\nu_2||a^{\mathrm{s}}_2|}\,. \tag{50}$$

The estimated saturation levels displayed in Fig. 6 by horizontal dashed lines agree well with the calculation results. Thus, the interacting wave amplitudes are nonlinearly maintained at a constant level within the beam, i.e., in the parametric decay region. However, due to the losses of the daughter wave energy from the microwave beam 'spot', their energy increases in the 2D volume where the numerical solution was obtained. We can calculate the anomalously absorbed power by analyzing the computation results.

Figure 9 displays the evolution of energy of all daughter plasmons in the 2D volume (in dimensionless units). It can be seen that as the saturation is reached, the daughter plasmon energy in the volume continues to grow, which is related to the losses of the daughter waves from the decay region. The relative pump wave power transferred to the daughter waves can be found using the numerical simulation results:

$$\frac{\Delta P}{P_0} = \frac{T_{\mathrm{e}}}{P_0}\frac{\partial}{\partial t}\int_{-y_{\mathrm{B}}}^{y_{\mathrm{B}}}\int_{-z_{\mathrm{B}}}^{z_{\mathrm{B}}}\frac{\mathrm{d}y\,\mathrm{d}z}{\pi d^2}\left(|a_1|^2 + |a_2|^2 + |a'_1|^2 + |a'_2|^2\right). \tag{51}$$

The obtained analytic estimate predicts the dependence of the anomalous absorption of the pump wave $\Delta P/P_0$ on its power in the form $\Delta P/P_0 \propto 1/\sqrt{P_0}$, which is confirmed by simulation results.

Figure 10 shows the dependence obtained by processing the numerical solution of system (51). The numerical simulation results (dots) are reproduced with good accuracy by the dependence $1/P_0^{1/2}$ (dashed curve). This allows estimating the fraction of power lost by the extraordinary wave beam due to nonlinear effects. For the discharge parameters used in the calculation and the microwave beam power 600 kW, up to 10% of the power is absorbed abnormally, i.e., transferred to various daughter UH and IB waves.

2.3 Calculation of the detected signal power and spectrum

Nonlinear interaction (merging) of various daughter UH waves excited as a result of cascade saturation of the primary low-threshold two-plasmon instability of an extraordinary wave may result in the generation of electromagnetic waves whose frequencies are shifted down relative to that of the pump wave. This mechanism allows explaining the anomalous scattering effect, which has been observed in many installations [67–72]. We now discuss this effect in more detail. In analyzing instability saturation in Section 2.2, we considered a cascade consisting of two sequential decays of a pump wave. In fact, the decay cascade can continue at a relatively small amplitude of the UH waves, as long as the 'depth' of the local maximum of the density profile allows the excited secondary UH wave to be localized in the direction of inhomogeneity.

Figure 11 shows the behavior of the absolute value of the radial wavenumber of daughter UH waves excited as a result

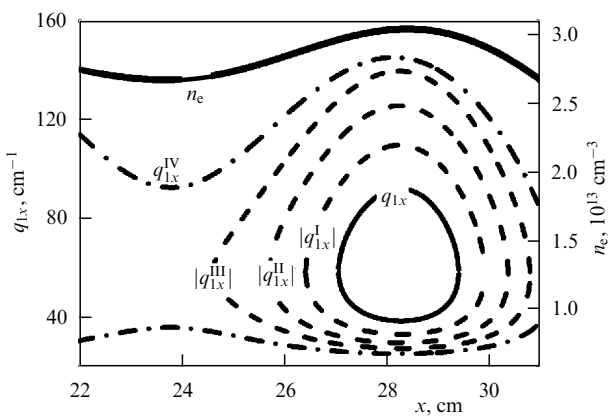

Figure 11. Dispersion curves of the primary UH wave (solid closed curve, the $m = 6$ mode), secondary UH waves (dashed curves, modes $m' = 16$, $m'' = 33$, and $m''' = 57$), and the secondary nonlocalized UH wave (dashed-dotted curve). The density profile (right vertical axis) is shown by the bold solid line.

of a decay cascade. The first three decays of the primary wave (solid line) are seen to lead to the excitation of localized UH waves (dashed lines). In the fourth decay, only a nonlocalized UH wave (dashed-dotted line) can be excited. However, its excitation threshold cannot be exceeded at a technologically available pump wave power, which breaks the chain of sequential decays.

We note that both primary daughter waves (41) decay, the only difference being that after the decay of one of them, UH and IB waves are excited that propagate in the direction opposite to the secondary waves generated as a result of the decay of the other. The merging of various UH waves during a three-stage cascade saturation of the primary instability results in the excitation of various extraordinary polarization waves. However, only nonlinearly generated electromagnetic waves with the frequencies

$$\frac{\omega_2+\omega_1'}{2\pi}=138.96\ \text{GHz}\,,\qquad \frac{\omega_2+\omega_1''}{2\pi}=138.44\ \text{GHz}\,,\qquad \frac{\omega_2+\omega_1'''}{2\pi}=137.92\ \text{GHz} \tag{52}$$

can propagate outward and be detected by sensors for diagnosing collective Thomson scattering; the frequency values reproduce the measured radiation spectrum with a reasonable accuracy (see Fig. 9 in [70]). We next focus on the first frequency line $(\omega_2+\omega_1')/(2\pi)=138.96$ GHz and calculate the amplitude of the signal recorded by the receiving antenna. According to [109], this amplitude can be represented as

$$A(\omega_\mathrm{a})=\frac{1}{4}\int \mathbf{j}_\mathrm{s}(\omega_\mathrm{a},\mathbf{r})\mathbf{E}^+(\omega_\mathrm{a},\mathbf{r})\,\mathrm{d}\mathbf{r}\,. \tag{53}$$

Formula (53) has a transparent physical meaning: it serves as one of the possible statements of the reciprocity theorem. It relates the contribution of a given point $\mathbf{r}$ to forming the radiation signal described by the current density $\mathbf{j}_\mathrm{s}(\omega_\mathrm{a})$ and the capacity of the same antenna, if it operates in the radiation mode ($\mathbf{E}^+$ is the field of the antenna beam of unit power), to illuminate this point $\mathbf{r}$ in the plasma with the inverted direction of the external magnetic field. Integration is performed in Eqn (53) over the entire plasma volume. In the nonlinear interaction region, the field $\mathbf{E}^+$ can be represented in the WKB approximation as [93]

$$\mathbf{E}^+=\sqrt{\frac{\omega_\mathrm{a}}{ck_{\mathrm{a}x}(x)}}\,\frac{\mathbf{e}^+(\omega_\mathrm{a})E_\mathrm{a}^+(y,z)}{2}\times\exp\left(\mathrm{i}\omega_\mathrm{a}t-\mathrm{i}\int^x k_{\mathrm{a}x}(x',K_\mathrm{a})\,\mathrm{d}x'-\mathrm{i}K_\mathrm{a}y\right)+\text{c.c.}\,, \tag{54}$$

where the initial distribution has the Gaussian shape

$$E_0^+(y,z)=\sqrt{\frac{8\pi}{c\pi d_\mathrm{a}^2}}\exp\left[-\frac{(y-y_\mathrm{a})^2+z^2}{2d_\mathrm{a}^2}\right],$$

where $y_\mathrm{a}=a\sin\theta$ is the vertical shift of the receiving antenna with respect to the equatorial plane (see Fig. 1), d_a is the receiving antenna size, $\omega_\mathrm{a}/(2\pi)$ is the signal frequency, $\mathbf{e}^+(\omega_\mathrm{a})=\mathbf{e}^*(\omega_\mathrm{a})$ is the polarization vector (see (12)), $k_{\mathrm{a}x}(x,K_\mathrm{a})=(k_0^2(x)-K_\mathrm{a}^2)^{1/2}$ is the wavevector component along the direction of inhomogeneity, $k_0(x)$ is the transverse component of the wavevector (see (14)), $K_\mathrm{a}=\omega_\mathrm{a}\sin\theta/c$, and θ is the angle of inclination of the receiving antenna. The convolution of the current density $\mathbf{j}_\mathrm{s}(\omega_\mathrm{i},\mathbf{r})$ excited as a result of the nonlinear interaction of the primary $\phi_1(\mathbf{r})$ and secondary $\phi_1'(\mathbf{r})$ UH waves (which describes the generation of an extraordinary wave propagating outward) with the polarization vector $\mathbf{e}^+(\omega_\mathrm{a})$ can be represented as (see Eqns (18) and (19))

$$e_k^+(\omega_\mathrm{a})\,j_{sk}(\omega_\mathrm{a})=-\mathrm{i}\,\frac{\omega_\mathrm{a}}{4\pi H}\,\chi_\mathrm{e}^{\mathrm{nl}*}\phi_2^*\phi_1'\,, \tag{55}$$

where the coefficient $\chi_\mathrm{e}^{\mathrm{nl}*}$ is defined in (19). We substitute (54) and (55) in (53) and integrate over the plasma volume. As a result, we first obtain the amplitude A of the recorded signal at a frequency of 138.96 GHz and then its power [93]:

$$p_\mathrm{s}(\omega_\mathrm{a})=\left|A(\omega_\mathrm{a})\right|^2=\sigma_\mathrm{a}\sigma_\mathrm{c}\,\frac{T_\mathrm{e}}{\tau_\mathrm{eff}}\,, \tag{56}$$

where $1/\tau_\mathrm{eff}=4\omega_\mathrm{a}^2T_\mathrm{e}/(cd_a^2H^2)$,

$$\sigma_\mathrm{a}=\left|\int_{-\infty}^{\infty}\frac{\mathrm{d}y\,\mathrm{d}z}{\pi d^2}\,a_2^*(y,z)a_1'(y,z)\times\exp\left[-\mathrm{i}K_\mathrm{a}y-\frac{(y-y_\mathrm{a})^2+z^2}{2d_\mathrm{a}^2}\right]\right|^2$$

is the angular resolution of the receiving antenna, and

$$\sigma_\mathrm{c}=\frac{1}{\omega_2\langle D_{2\omega}\rangle\omega_1'\langle D_{1\omega}'\rangle}\left|\int_{-\infty}^{\infty}\mathrm{d}x\sqrt{\frac{\omega_\mathrm{a}}{ck_{\mathrm{a}x}(x)}}\,\frac{\chi_\mathrm{e}^{\mathrm{nl}}(x)}{\sqrt{L_n^-(x)}\sqrt{L_m'^+(x)}}\times\exp\left(\mathrm{i}\int^x\left(q_x^+(m,\xi)-q_x^-(n,\xi)-k_{\mathrm{a}x}(\xi,K_\mathrm{a})\right)\mathrm{d}\xi\right)\right|^2,$$

where m and n are the number of the radial modes of localized UH waves, describes the efficiency of nonlinear interaction (merging) between UH waves. Next, to estimate the radiative temperature, we calculate the integrals in Eqn (56) using the distributions $a_2(y,z)$ and $a_1'(y,z)$ obtained from the solution of the system of equations that describe cascade saturation of the primary absolute instability with the pump wave depletion taken into account. As a result of numerical integration, we obtain the following estimate for the radiation temperature:

$$\frac{p_\mathrm{s}(\omega_\mathrm{a})}{\Delta\nu}=0.8\ \text{MeV}\,, \tag{57}$$

where $\Delta\nu\approx 0.15$ GHz is the spectral width of the frequency line, whose value was obtained by analyzing the experimental spectra. Estimate (57) is close to the measured radiative temperature $p_\mathrm{s}(\omega_\mathrm{a})/\Delta\nu\approx 1$ MeV (see Figs 9 and 11 in [70]). It can be noted in analyzing formula (56) that $p_\mathrm{s}(\omega_\mathrm{a})/\Delta\nu\propto P_0^2$ [93]. As shown in Fig. 12, this dependence is in reasonable agreement with the experimental data obtained in [67].

Thus, the developed theoretical model describes low-threshold excitation in the vicinity of a local maximum of the nonmonotonic density profile of two confined UH waves. This model enables the reproduction with reasonable accuracy of both the spectrum of anomalous radiation and its radiation temperature, which were measured in [67, 70].

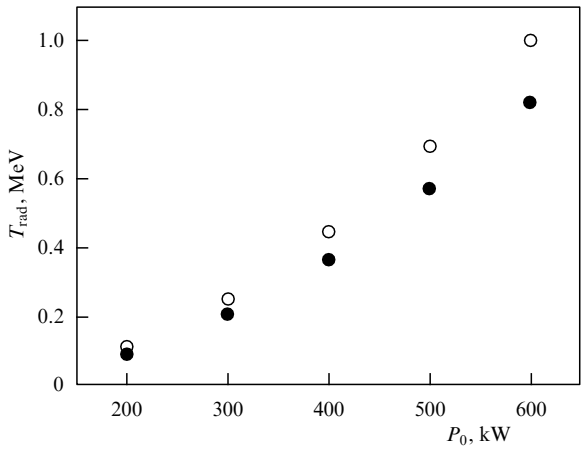

Figure 12. Radiation temperature measured in the experiment (unfilled circles) [67] and predicted by the analytical model (56) (filled circles) as a function of microwave beam power.

Driven by this agreement between theory and experimental data, we have to give full attention to the predicted significant anomalous absorption of microwave power due to the excitation of daughter waves. (For the decay cascade illustrated in Fig. 11, up to 25% of the pump wave power is 'input' into the generated UH waves.)

The low-frequency IB waves excited in the decay process leave the nonlinear interaction region to be subsequently absorbed by ions near the nearest harmonic of the ion cyclotron resonance. This may result in a distortion of the ion distribution function, which provides a qualitative explanation of the generation of a high-energy ion group observed under auxiliary ECRH of plasma in various installations [73–76].

The propagation paths of the generated daughter UH waves differ significantly from those of the microwave pump beam. They are absorbed by electrons far from the plasma column areas that were predicted in the approach based on the linear behavior of the pump wave. The difference between the energy release profile and that predicted in the linear approximation may be at least partially responsible for the nonlocal heat transfer in the electron channel observed in many experiments [58].

3. Parametric decay of an extraordinary wave with excitation of a single localized upper hybrid plasmon

3.1 Primary instability

We note that the concurrent parametric excitation of two UH waves confined in the direction of a plasma inhomogeneity, which is considered in Section 2, is a relatively rare event because it not only requires the existence of a nonmonotonic density profile but also imposes stringent conditions on the density in the local maximum and minimum. In this section, we consider two-plasmon decay in a more frequent case where only one of the parametrically excited UH waves is confined in the vicinity of a local maximum density. We assume in this case that the pump wave propagates at an angle to the external magnetic field. In the vicinity of the decay region, we can ignore the effects of the magnetic field shear and the magnetic surface curvature and, as in Section 2, use a Cartesian coordinate system (x, y, z). In the chosen coordinate system, the pump wave field can be represented in the WKB approximation in form (11) where

$$k_{0x}(x) \simeq \frac{\omega_0}{c}\sqrt{\frac{\varepsilon_0^2 - g_0^2}{\varepsilon_0}}\left(1 + \frac{k_{0z}^2 c^2}{2\omega_0^2}\,\frac{\eta_0}{g_0^2}\right). \tag{58}$$

We consider parametric excitation of the longitudinal UH waves $\phi_1 \propto \exp(-\mathrm{i}\omega_1 t)$ and $\phi_2 \propto \exp[\mathrm{i}(\omega_0 - \omega_1)t]$ by pump wave (11). If the density profile is not monotonic, one of these UH waves can be confined in the direction of inhomogeneity. Its potential in the absence of a pump wave is given by Eqn (20), and its eigenfrequency $\omega_1 = \omega^m$ satisfies a quantization condition similar to (23). The potential of the second daughter wave, whose frequency is $\omega_2 = \omega_0 - \omega^m$, can be represented in the WKB approximation in the absence of the pump wave as

$$\phi_2 = \frac{C_2}{\sqrt{D_{2q}}}\exp\left(\mathrm{i}\int^x q_{2x}(x', q_{2z})\,\mathrm{d}x' + \mathrm{i}q_{2z}z + \mathrm{i}\omega_2 t\right) + \text{c.c.}\,, \tag{59}$$

where $q_{2z} = k_{0z}$, $C_2 = \text{const}$, $D_{2q} = |\partial D_2/\partial q_{2x}|_{q_x}$, and $q_{2x} = q_{2x}(q_{2z}, x)$ is a solution of the local dispersion relation $D_2 = D_{\rm UH}(\omega_2, q_{2x}, q_{2z}) = 0$. The explicit form of q_{2x} is given by a formula similar to (22).

Figure 13 displays the dispersion curves of the waves involved in nonlinear interaction under the conditions of ECRH experiments [67, 70]: the solid curve shows the localized UH-wave wavenumber shifted upward by the pump-wave wavenumber $q_{1x} + k_{0x}$, while the dashed line shows the wavenumber of the second daughter wave. It can be seen that as a result of the parametric decay of the pump wave in the vicinity of the intersection points of these curves, a UH wave and a slow UH wave that leaves the nonlinear interaction region along the direction of inhomogeneity are excited in the vicinity of the local maximum of the density profile. Due to the nonlinear interaction, the daughter wave amplitudes are no longer constant, i.e., $C_2 \to C_2(\mathbf{r}, t)$ and $C_m \to C_m(y, z, t)$. Their behavior is described by the system of two partial differential equations [94]

$$\begin{aligned}
&\left(\frac{\partial}{\partial t} + v_{2x}\frac{\partial}{\partial x} + \mathrm{i}\Lambda_{2y}\frac{\partial^2}{\partial y^2} + v_{2z}\frac{\partial}{\partial z}\right)C_2 = -C_m\chi_{\rm e}^{\rm nl}\,\frac{E_{\rm i}(y,z)}{2H}\\
&\quad\times\frac{\varphi_m(x)}{D_{2\omega}}\sqrt{\frac{\omega_0 D_{2q}(x)}{ck_{0x}(x)}}\exp\left[\mathrm{i}\int^x\big(k_{0x}(x') - q_{2x}(x')\big)\,\mathrm{d}x'\right],\\
&\left(\frac{\partial}{\partial t} + \mathrm{i}\Lambda_{my}\frac{\partial^2}{\partial y^2} + \mathrm{i}\Lambda_{mz}\frac{\partial^2}{\partial z^2}\right)C_m = \frac{\chi_{\rm e}^{\rm nl*}}{\langle D_{1\omega}\rangle}\,\frac{E_{\rm i}^*(y,z)}{2H}\\
&\quad\times\int_{-\infty}^{\infty}\mathrm{d}x\sqrt{\frac{\omega_0}{ck_{0x}(x)D_{2q}(x)}}\,C_2(x)\varphi_m^*(x)\\
&\quad\times\exp\left[\mathrm{i}\int^x\big(q_{2x}(x') - k_{0x}(x')\big)\,\mathrm{d}x'\right].
\end{aligned} \tag{60}$$

In deriving Eqns (60), we used the averaging procedure in (24) and adopted the following notation: v_{2x} and v_{2z} are the group velocity components, Λ_{2y} is the diffraction coefficient of the second daughter wave, Λ_{my} and Λ_{mz} are the diffraction coefficients of the UH wave confined along the direction of inhomogeneity, and the nonlinear coupling coefficient $\chi_{\rm e}^{\rm nl}$ is given by formula (19). In addition, because we can disregard

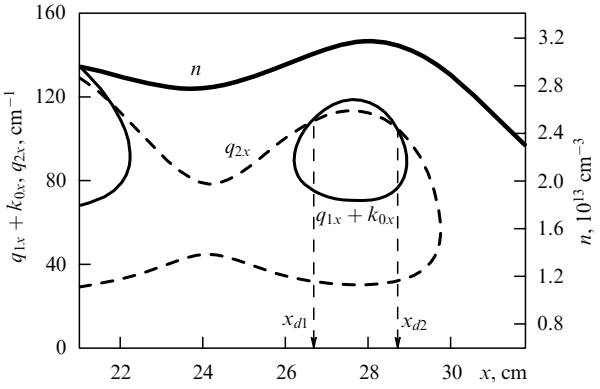

Figure 13. Unconfined UH wave dispersion curve q_{2x} (dashed line) and the localized UH wave dispersion curve ($m = 9$, $f_1 = 70.47$ GHz) shifted upward by the wave wavenumber $q_{1x} + k_{0x}$ ($f_0 = 140$ GHz, $k_{0z} = 2.55$ cm^{-1}) (solid line). The solid bold curve shows the density profile in the presence of a magnetic island.

the pump wave depletion in describing the primary instability, we assume that its amplitude depends only on the transverse coordinates and is determined by the boundary conditions, i.e., $E_{\rm i}(x,y,z) \to E_{\rm i}(y,z) = E_{\rm i}(x,y,z)|_{x\to-\infty}$.

Furthermore, we assume that the instability growth rate γ is much smaller than the inverse time τ of the convective and diffraction losses by the second daughter wave in the decay region:

$$\gamma\tau \ll 1\,. \tag{61}$$

We use this inequality below to check the validity of our assumption after clarifying the possibility of exciting absolute instability and determining its growth rate. For the parametric decay shown in Fig. 13, the main energy loss of the nonconfined daughter wave is its loss along the direction of inhomogeneity. In this case, in the left-hand side of the first equation in (60), we can keep only the term that describes the wave convection in the direction x,

$$v_{2x}\,\frac{\partial}{\partial x}\,C_2 = -C_m\chi_{\rm e}^{\rm nl}\,\frac{E_{\rm i}(y,z)}{2H}\,\frac{\varphi_m(x)}{D_{2\omega}}\sqrt{\frac{\omega_0 D_{2q}(x)}{ck_{0x}(x)}} \times \exp\left[{\rm i}\int^x \big(k_{0x}(x') - q_{2x}(x')\big)\,{\rm d}x'\right]. \tag{62}$$

We integrate Eqn (62), taking the boundary condition $C_2|_{x\to\infty} = 0$ into account. We thus obtain the amplitude of the second daughter wave as

$$C_2 = \frac{E_{\rm i}(y,z)}{2H}\,C_m\int_x^\infty {\rm d}x'\sqrt{\frac{\omega_0}{ck_{0x}(x')D_{2q}(x')}}\,\chi_{\rm e}^{\rm nl}(x') \times \varphi_m(x')\exp\left[{\rm i}\int^{x'}\big(k_{0x}(x'') - q_{2x}(x'')\big)\,{\rm d}x''\right]. \tag{63}$$

Substituting Eqn (63) in the right-hand side of the second equation in (60), we arrive at the following equation for the amplitude of the UH wave confined in the direction of inhomogeneity in the vicinity of a local maximum of the plasma density profile [94]:

$$\left(\frac{\partial}{\partial t} + {\rm i}\Lambda_{my}\,\frac{\partial^2}{\partial y^2} + {\rm i}\Lambda_{mz}\,\frac{\partial^2}{\partial z^2}\right)a_1 = v_0(y,z)a_1\,, \tag{64}$$

where the nonlinear amplification factor is

$$v_0 = \frac{\big|E_{\rm i}(y,z;P_0)\big|^2}{4H^2\big\langle D_{1\omega}(\omega^m)\big\rangle}\int_{-\infty}^\infty {\rm d}x\sqrt{\frac{\omega_0}{ck_{0x}(x)D_{2q}(x)}}\,\varphi_m^*(x)\chi_{\rm e}^{\rm nl}(x) \times \int_x^\infty {\rm d}x'\sqrt{\frac{\omega_0}{ck_{0x}(x')D_{2q}(x')}}\,\varphi_m(x')\chi_{\rm e}^{\rm nl}(x') \times \exp\left[{\rm i}\int_x^{x'}\big(k_{0x}(x'') - q_{2x}(x'')\big)\,{\rm d}x''\right]. \tag{65}$$

In Eqn (65), we used the normalization of the amplitude similar to normalization (27).

It is noteworthy that in contrast to the parametric decay of a pump wave into two localized UH waves, the parametric instability under consideration is described by a single partial differential equation with variable coefficients. We show in what follows that this equation has particular solutions that grow exponentially in time, i.e., that it describes absolute instability. We represent the sought UH wave amplitude in the form

$$a_1 = a_{10}\exp(\gamma t)\,, \tag{66}$$

where a_{10} is a function of coordinates. Substituting (66) in (64), we obtain an equation for the amplitude a_{10}:

$$\left(\gamma + {\rm i}\Lambda_{my}\,\frac{\partial^2}{\partial y^2} + {\rm i}\Lambda_{mz}\,\frac{\partial^2}{\partial z^2}\right)a_{10} = v_0(y,z)a_{10}\,. \tag{67}$$

If the pump wave power is so large that the nonlinear amplification of the daughter UH wave localized in the direction of the inhomogeneity is much greater than the diffraction loss of its energy in the nonlinear interaction region, i.e., $\Lambda_{1y,z}/(\pi d^2) \ll v_0$, we can expand the coefficient in the right-hand side of (67) in a series, $v_0(y,z) = v_0(0,0) - v_0(0,0)(y^2+z^2)/d^2$, to obtain the equation [94]

$$\left({\rm i}\Lambda_{my}\,\frac{\partial^2}{\partial y^2} + {\rm i}\Lambda_{mz}\,\frac{\partial^2}{\partial z^2} + \gamma - v_0 + v_0\,\frac{y^2}{d^2} + v_0\,\frac{z^2}{d^2}\right)a_{10} = 0\,, \tag{68}$$

which has the form of the stationary Schrödinger equation with a complex-valued parabolic potential. Unless indicated otherwise, in Eqn (68) and below, $v_0(0,0) \to v_0$. A particular solution of Eqn (68) is given by the eigenfunctions $\psi_s(y)$ and $\psi_r(z)$ expressed in terms of the Hermite polynomials,

$$\psi_t(\xi) = \exp\left(-\frac{\xi^2}{2\delta_\xi^2}\right)H_t\left(\frac{\xi}{\delta_\xi}\right) \tag{69}$$

with $t = s, r$, and $\xi = y, z$; here, H_t is a Hermite polynomial and

$$\delta_\xi = \frac{\Lambda_{m\xi}^{1/4}\,d^{1/2}\,\exp\left(-{\rm i}\pi/8 - {\rm i}\arg v_0/4\right)}{v_0^{1/4}}\,.$$

Thus, the approximate solution of Eqn (64) describes a UH wave that is localized along the coordinates y and x (i.e., on a magnetic surface within a microwave beam) [94]:

$$a_1 = \exp\left(\gamma_{s,s}t + {\rm i}\delta\omega_{s,s}t\right)\psi_s(y)\psi_r(z)\,. \tag{70}$$

The growth rate and correction to the frequency of this wave are found from the quantization condition and can be

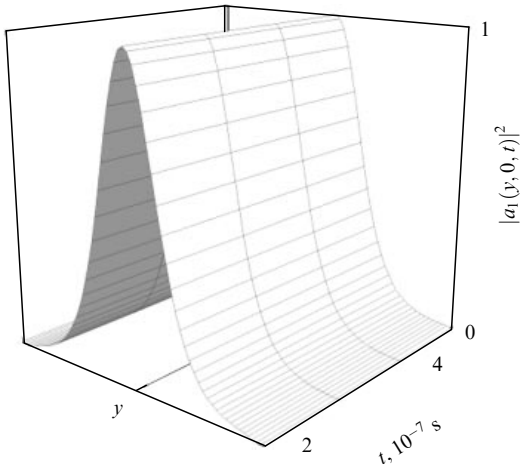

Figure 14. Evolution of the UH wave energy distribution $|a_1(y,0,t)|^2$ along the coordinate y found by solving Eqn (64) numerically.

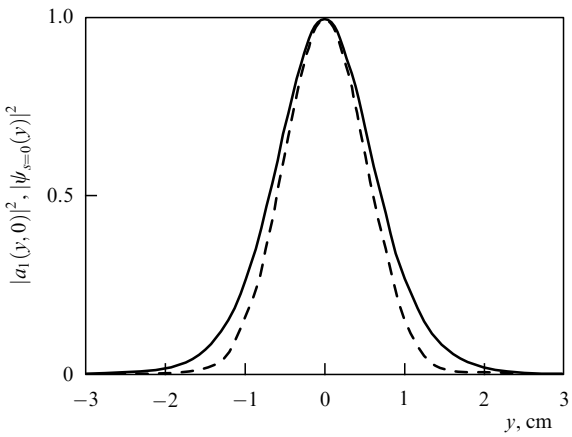

Figure 15. Comparison of the UH wave energy distribution $|a_1(y,0,t_0)|^2$ (solid curve) at the moment $t_0 = 5\times10^{-7}$ s with the analytic solution $|\psi_s(y)|^2$, $s = 0$ (see (69)), which is shown by the dashed line.

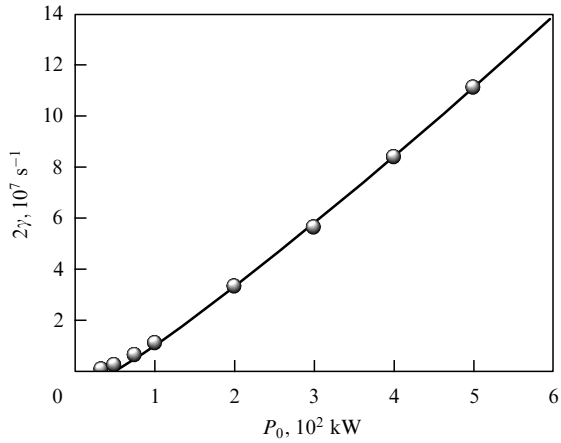

Figure 16. Instability growth rate as a function of the pump wave power. The circles show a numerical solution of Eqn (64) for the experimental conditions [67, 70]. The solid curve corresponds to formula (71). $P_0^{\rm th} = 37$ kW.

expressed explicitly as [94]

$$\begin{pmatrix}\gamma_{s,r}\\ \delta\omega_{s,r}\end{pmatrix} = \begin{pmatrix}v_0'\\ v_0''\end{pmatrix} - \begin{pmatrix}\cos\left(\dfrac{\arg v_0}{2}-\dfrac{\pi}{4}\right)\\ \sin\left(\dfrac{\arg v_0}{2}-\dfrac{\pi}{4}\right)\end{pmatrix} \times\sqrt{|v_0|}\left[(2s+1)\sqrt{\frac{\Lambda_{my}}{w^2}}+(2r+1)\sqrt{\frac{\Lambda_{mz}}{w^2}}\right]. \quad (71)$$

The threshold of parametric instability accompanied by the generation of a 3D-localized UH wave is determined by the equation [94]

$$v_0'(P_0^{\rm th}) = \cos\left(\frac{\arg v_0(P_0^{\rm th})}{2}-\frac{\pi}{4}\right)\sqrt{|v_0(P_0^{\rm th})|} \times\left[(2s+1)\sqrt{\frac{\Lambda_{my}}{d^2}}+(2r+1)\sqrt{\frac{\Lambda_{mz}}{d^2}}\right]. \quad (72)$$

Next, we solve Eqn (64) numerically. The results of the numerical solution obtained for the parametric decay displayed in Fig. 13 are shown in Figs 14–16. Figure 14 represents the spatial distribution of the UH wave energy along the y direction. It can be seen that the shape of the $|a_1(y,0,t)|^2$ distribution does not change in time, which indicates that an eigenfunction of this equation is excited. Figure 15 compares the distribution $|a_1(y,0,t_0)|^2$ (solid curve) at $t_0 = 5\times10^{-7}$ s with the analytic solution $|\psi_s(y)|^2$ (see Eqn (69)) for the fundamental mode $s = 0$, which is shown by a dashed curve. Similarly, the shape of the wave energy distribution $|a_1(0,z,t)|^2$ along the magnetic field does not change in time either and is described well by the analytic dependence.

Thus, the numerical solution indicates the excitation of the UH wave eigenmodes localized within the microwave beam. The amplitude of these modes increases exponentially with growth rate given by (71) (see Fig. 16), which indicates the excitation of absolute decay instability. The instability threshold determined from the computation is in agreement with the value $P_0^{\rm th} = 37$ kW that can be obtained analytically from Eqn (72). Because the characteristic time for which the second unconfined daughter wave leaves the nonlinear interaction region is of the order of $\tau \approx 0.5\times(10^{-8}-10^{-9})$ s (depending on the parameters), assumption (61) that was used to describe the convective losses of its energy is valid. At the same time, the instability growth rate is such that the excited localized UH waves undergo a significant increase from the thermal fluctuation level. Most likely, the parametric decay instability is saturated due to the secondary instability of the daughter UH wave. We discuss this process in Section 3.2 and evaluate the saturation levels of daughter waves and the proportion of power lost by the microwave beam.

3.2 Saturation of the instability

We consider the saturation of the decay instability of the pump wave as a result of the secondary low-threshold decay of the primary localized UH wave. If a local density maximum is sufficiently high, it is natural to expect that the primary UH wave decays into a secondary UH wave, localized, like the primary wave, in the direction of inhomogeneity in the vicinity of the local density maximum, and the IB wave that freely propagates along the x coordinate. To analyze the saturation mechanism from a conceptual perspective, we explore only the secondary instability, disregarding higher-order parametric processes.

The equation for the amplitude a_1' of the secondary UH wave eigenmode p (see Eqn (41)) can be obtained similarly to Eqn (42) in the form [100]

$$\left(\frac{\partial}{\partial t}+\mathrm{i}\Lambda_{py}\frac{\partial^2}{\partial y^2}+\mathrm{i}\Lambda_{pz}\frac{\partial^2}{\partial z^2}\right)a_1'=v_1\sqrt{\frac{\omega^p}{\omega^m}}\,|a_1|^2a_1'\,,$$

where Λ_{py} and Λ_{pz} are the diffraction coefficients of the mode p, and v_1 is the nonlinear coupling coefficient defined in Eqn (43). If the secondary decay of the primary wave is taken into account in Eqn (64), the system of equations that describe the two-step cascade decay of the pump wave becomes [100]

$$\begin{gathered}\left(\frac{\partial}{\partial t}+\mathrm{i}\Lambda_{my}\frac{\partial^2}{\partial y^2}+\mathrm{i}\Lambda_{mz}\frac{\partial^2}{\partial z^2}\right)a_1=v_0(y,z)a_1-v_1\sqrt{\frac{\omega^m}{\omega^p}}\,|a_1'|^2a_1\,,\\ \left(\frac{\partial}{\partial t}+\mathrm{i}\Lambda_{py}\frac{\partial^2}{\partial y^2}+\mathrm{i}\Lambda_{pz}\frac{\partial^2}{\partial z^2}\right)a_1'=v_1\sqrt{\frac{\omega^p}{\omega^m}}\,|a_1|^2a_1'\,.\end{gathered}\tag{73}$$

In the case of a plane pump wave, i.e., $d\to\infty$, $v_0(y,z)\to v_0(0,0)$, the solution of system of equations (73) is given by multicomponent cnoidal waves [107, 108]. These solutions describe the transition of interacting waves from the exponential growth mode to a strongly nonlinear oscillatory mode, in which the frequency of their oscillations depends on the amplitude of all the oscillations involved in the interaction. The situation is radically different in the realistic case of a finite-width beam. We demonstrate this below, primarily by numerically solving system of nonlinear partial differential equations (73).

As in Section 2, we use the finite difference method and a 2D integration region $2y_{\mathrm{B}}\times 2z_{\mathrm{B}}$ whose dimensions are much larger than the microwave beam size (i.e., the nonlinear interaction region), $y_{\mathrm{B}}, z_{\mathrm{B}}\gg d$. In addition, we use periodic boundary conditions and typical parameters of ECRH experiments [67, 70]. The obtained solution is shown in Fig. 17, where the evolution of the energy density of primary $\langle|a_1(t)|^2\rangle_{\mathrm{pdi}}$ (solid curve) and secondary $\langle|a_1'(t)|^2\rangle_{\mathrm{pdi}}$ (dashed curve) plasmons in the beam 'spot' (see the averaging procedure (47)) is displayed. It can be seen that the primary instability develops initially. The primary UH wave energy increases in this case exponentially. This increase is described well by the linear dependence $2\gamma t$ (dashed-dotted line), where the growth rate γ is defined in Eqn (71), $s, r=0$. At about $t\approx 2.3\times 10^{-7}$ s, the primary wave energy exceeds the secondary instability threshold. This leads to an exponential increase in the secondary UH wave energy density. As a result, the system relaxes to a quasistationary state.

Thus, we have shown that system of equations (73) admits a stationary solution in the case of a spatially bounded pump wave. We can estimate the saturation levels of the corresponding UH waves based on the following energy considerations. The energy density of the primary plasmons should compensate the loss of the secondary plasmons from the microwave beam 'spot' and drive the secondary instability to virtually the excitation threshold

$$|a_1^{\mathrm{s}}|^2\approx\frac{1}{\tau_1' v_1}\,,\tag{74}$$

where $\tau_1'=\pi d^2/\max(\Lambda_{py},\Lambda_{pz})$ is the time scale that characterizes the rate of secondary wave energy loss in the decay region. The secondary plasmon energy density in the decay region in the saturation mode should be such that the primary

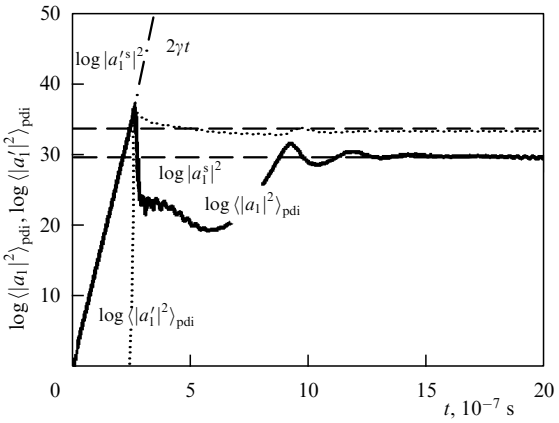

Figure 17. Evolution of the energy density of daughter primary $\langle|a_1(t)|^2\rangle_{\mathrm{pdi}}$ (solid curve) and secondary $\langle|a_1'(t)|^2\rangle_{\mathrm{pdi}}$ (dashed curve) UH plasmons in the microwave beam 'spot'. The dashed-dotted line shows the analytic expression $2\gamma t$, where the growth rate γ is given by Eqn (71). The horizontal dashed lines are estimates of saturation levels (74) (bottom line) and (75) (top line).

instability be maintained near the excitation threshold due to nonlinear dissipation, i.e.,

$$|a_1'^{\mathrm{s}}|^2\simeq\frac{|v_0(0,0)|}{v_1}\,.\tag{75}$$

The obtained estimates of saturation levels displayed in Fig. 17 as horizontal dashed lines show good agreement with the results of numerical calculations.

Thus, we have shown both numerically and analytically that system of equations (73) admits a stationary solution that can be interpreted as the saturation mode of parametric decay instability. The daughter wave energy losses from the microwave beam 'spot,' where the interacting wave amplitudes are nonlinearly maintained at a constant level, result in this case in an increase in their energy in a 2D volume $2y_{\mathrm{B}}\times 2z_{\mathrm{B}}$. We can analytically estimate the proportion of the pump wave power lost in the parametric decay:

$$\Delta P_0=\frac{T_{\mathrm{e}}}{\tau_1}\langle|a_1^{\mathrm{s}}|^2\rangle_{\mathrm{pdi}}+\frac{T_{\mathrm{e}}}{\tau_1'}\langle|a_1'^{\mathrm{s}}|^2\rangle_{\mathrm{pdi}}\,,\tag{76}$$

where $\tau_1=\pi d^2/\max(\Lambda_{my},\Lambda_{mz})$ is the time scale that characterizes the rate of primary wave energy loss in the decay region. If the microwave beam power significantly exceeds the excitation threshold of the primary instability (see Eqn (72)), the second term dominates in Eqn (76):

$$\Delta P_0\approx\frac{T_{\mathrm{e}}}{\tau_1'}\langle|a_1'^{\mathrm{s}}|^2\rangle_{\mathrm{pdi}}\propto P_0\,,\tag{77}$$

which describes the power input to the secondary UH waves. Because $\Delta P_0\propto P_0$, the proportion of anomalously absorbed power does not depend on the pump wave power and is only determined by the efficiency of the nonlinear coupling between the interacting waves in the first and second decay, $\Delta P_0/P_0\approx|v_0(0,0;P_0\leftrightarrow T_{\mathrm{e}}/\tau_1')|/v_1$, where the microwave beam power in formula (65) for v_0 should be replaced with T_{e}/τ_1', $P_0\to T_{\mathrm{e}}/\tau_1'$. The accurate value of the anomalous absorption efficiency can be obtained from an analysis of numerical calculations.

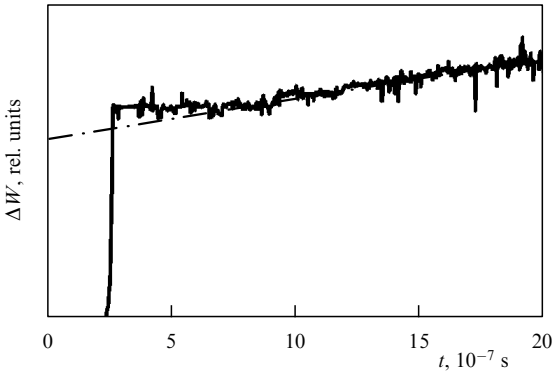

Figure 18. Evolution of the total energy of daughter plasmons (solid curve). The dashed-dotted line represents the linear behavior of the numerically obtained increase in total energy of UH waves in the 2D region, where the solution was sought, in the saturation mode.

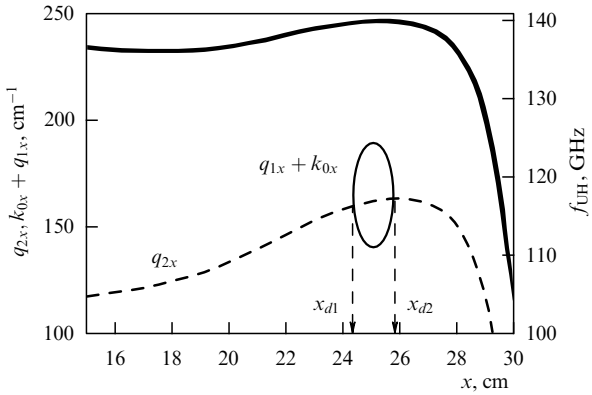

Figure 19. Dispersion curves of the electron plasma wave q_{2x} (dashed line) and the localized UH wave $q_{1x} + k_{0x}$ (solid line) ($m = 8$, $f_1 = 138.5$ GHz), which is shifted upward by the pump wave wavenumber ($f_0 = 140$ GHz, $k_{0z} = 2.55$ cm^{-1}). The upper hybrid frequency profile is shown by a solid bold curve [72].

Figure 18 shows the evolution of energy of all daughter plasmons

$$\Delta W = T_{\mathrm{e}} \int_{-y_{\mathrm{B}}}^{y_{\mathrm{B}}} \int_{-z_{\mathrm{B}}}^{z_{\mathrm{B}}} \frac{\mathrm{d}y\,\mathrm{d}z}{\pi d^2} \left(\left|a_1(y,z)\right|^2 + \left|a_1'(y,z)\right|^2 \right) \quad (78)$$

(in dimensionless units). It follows from the figure that if saturation is reached, the daughter UH plasmon energy in the volume continues to increase, which is associated with pumping out the daughter waves from the decay region. Figure 18 shows that this increase is approximated well by a linear dependence (dashed-dotted line), which indicates that the power transferred from the microwave beam to UH waves is constant. The proportion of the microwave beam power transferred to the daughter waves is

$$\frac{\Delta P}{P_0} = \frac{1}{P_0} \frac{\partial \Delta W}{\partial t} \,. \quad (79)$$

Formula (79) can be used to show that at the pump wave power $P_0 = (0.6-1)$ MW, the proportion of anomalously absorbed power does not change and is $\Delta P/P_0 \approx 16\%$ in the extraordinary wave decay (analytic estimate (77) yields $\Delta P/P_0 \approx 15.4\%$).

In concluding this section, we note that analytic dependences and energy estimates are in agreement with the numerical solution. This agreement provides confidence that the numerical solution is correct, and the estimates of the anomalous absorption of the microwave pump wave are reasonable.

4. Excitation of a localized upper hybrid plasmon in the parametric decay of an ordinary wave

The x component of the wavevector in formula (11) in the case of parametric decay of an ordinary polarized wave takes the form

$$k_{0x} \simeq \frac{\sqrt{\eta}\omega_0}{c\left[1 - k_{0z}^2 c^2/(2\omega_0^2)\right]} \,. \quad (80)$$

The components of the polarization vector $\mathbf{e}_0$ are determined from the Maxwell equations as

$$\frac{e_x}{e_y} = -\mathrm{i}\,\frac{\omega_{\mathrm{c}}}{\omega_0} \,, \qquad \frac{e_x}{e_z} \approx \sqrt{\eta} n_z \,, \quad (81)$$

where $n_z = k_{0z}c/\omega_0 = \sin\theta \ll 1$ is the longitudinal refractive index. The parametric decay of the pump wave may result in the excitation of a localized UH wave and an electron plasma (EP) wave, which rapidly leaves the decay region. The EP wave frequency belongs to the intermediate range $\omega_{\mathrm{ci}} \ll \omega_{\mathrm{pi}} < \omega_2 \ll \omega_{\mathrm{ce}}$, and the dispersion relation has the form

$$q_{2x} \simeq q_{2z}\sqrt{-\frac{\eta}{\varepsilon}} \,. \quad (82)$$

Figure 19 shows the possibility of a parametric decay of an ordinary wave, which leads to the excitation of UH wave resonances for typical conditions of ECRH experiments at the first harmonic of EC resonance [72]. The EP wave dispersion curve is shown in Fig. 19 by the dashed line. The dispersion curve of the UH wave ($n = 8$, $f_1 = 138.5$ GHz) localized in the vicinity of a local density maximum (bold solid line), shifted upward by the pump wave wavenumber $f_0 = 140$ GHz, $k_{0z} = 2.55$ cm^{-1}, is shown by the solid line ($q_{1x} + k_{0x}$). The decay resonance conditions are satisfied at the curve intersection points. It is in the vicinity of these points that ordinary polarization pump wave decay can occur. Due to nonlinear interaction, the amplitudes of daughter waves become coupled. Their interaction in the presence of a powerful microwave beam is described by system of equations (60), where the nonlinear coupling coefficient $\chi_{\mathrm{e}}^{\mathrm{nl}}$ can be found, according to [110], in the dipole approximation:

$$\chi_{\mathrm{e}}^{\mathrm{nl}} = \frac{\chi_{\mathrm{e}}(\omega_1)\chi_{\mathrm{i}}(\omega_2)}{q_{1x}q_{2x}} \sqrt{\frac{\omega_0}{ck_{0x}}}\, \frac{ck_{0z}\omega_{\mathrm{ce}}}{\omega_0^2}$$
$$\times \left[\left(1 + \frac{ck_{0x}\sqrt{\omega_0^2 - \omega_{\mathrm{pe}}^2}}{\omega_0^2 - \omega_{\mathrm{ce}}^2} \right) + \mathrm{i} \left(\frac{ck_{0x}\sqrt{\omega_0^2 - \omega_{\mathrm{pe}}^2}}{\omega_0^2 - \omega_{\mathrm{ce}}^2} \right) \right]. \quad (83)$$

Coefficient (83) contains a small parameter $ck_{0z}/\omega_0 \ll 1$, which reflects the low efficiency of the nonlinear coupling of an ordinary wave whose dominant electric field component is directed along the external magnetic field with the short-wave oscillations that primarily propagate across it.

The main energy loss of the EP wave in the case presented in Fig. 19 is convective energy transfer along the direction of inhomogeneity. The EP wave amplitude is described by the equation obtained from Eqn (63) by replacing the nonlinear susceptibility with formula (83). As shown in [96, 97], the evolution of the confined UH wave amplitude is described by

Eqn (64) with amplification factor (65) in which χ_e^{nl} is taken in form (83). A particular solution of Eqn (64) is a localized field distribution of the UH wave whose amplitude increases exponentially with time [96, 97]. According to the conclusions in [96, 97], the growth rate and threshold of this instability are described by formulas similar to (71) and (72). Because the efficiency of the nonlinear coupling of electrostatic oscillations with an ordinary wave is much lower than with an extraordinary wave, this instability threshold is much higher, $P_0^{th} = 173$ kW, and the growth rate is lower, $2\gamma = 5.88 \times 10^6$ s^{-1}, than in the case of extraordinary wave decay. However, for the pump wave power currently in use (up to 1 MW), this instability can be excited in experiments.

The ordinary wave decay instability is most probably saturated as a result of a cascade of primary localized UH wave decays [101]. The description of this mechanism is similar to that of the saturation mechanism of the primary decay instability of an extraordinary wave by system of equations (73). We do not discuss the details of the numerical solution of these equations or analytic estimates of the parameters of ECRH experiments at the fundamental harmonic of the resonance because such calculations are similar to those described in detail in Section 3. We now formulate the main results.

The primary instability is saturated as a result of the secondary instability of the UH wave. Daughter wave saturation levels are described well by analytic estimates (74) and (75). As a result of the excitation and saturation of ordinary wave instability, up to $\Delta P/P_0 \approx 4.7\%$ of the microwave beam power is lost in the generation of daughter waves (the analytic estimate yields $\Delta P/P_0 \approx 3.4\%$).

5. Conclusions

We presented the theory of low-threshold parametric decay instability of microwaves, which is based on the three-wave interaction model developed in pioneering studies [1–4]. The theory that goes beyond the well-established concepts popular in the 1980s–1990s [60–62] provides an explanation of the anomalous phenomena that have been observed in many thermonuclear toroidal magnetic traps during the propagation of high-power microwave beams widely used for EC plasma heating and the generation of induction-free drag currents. The theory has allowed reproducing the basic laws and characteristics of anomalous radiation, including its spectrum and radiation temperature, with reasonable accuracy [67, 70]. This theory makes it possible to qualitatively explain the effect of ion acceleration, which was observed in experiments on the ECRH of plasma at various facilities [73–76]. This agreement between theory and experimental data strongly substantiates the prediction of a significant anomalous absorption of the microwave beam power by daughter waves (from one tenth to a quarter of the total power) and shows ways in which the theory should be further developed.

However, although the very existence of a substantial anomalous absorption has been predicted, its magnitude is clearly insufficient to explain the significant broadening of the microwave beam energy profile observed at various installations [58, 59, 111–117]. Interpretation of experimental data requires further analysis of the strongly nonlinear mode of development of the parametric decay process and the search for scenarios wherein the instability saturation level increases significantly.

It is also necessary to analyze in detail the possibility of excitation and saturation scenarios of low-threshold parametric decay instabilities of microwave beams for the conditions of the ITER tokamak currently under construction and the DEMO installation, which need significantly higher EC plasma heating powers than those available in modern installations. Of great practical interest is also the study of options that can affect the anomalous absorption level in the development of low-threshold parametric decay instabilities by changing the diameter of the employed microwave beams.

The analysis of the development and saturation of low-threshold parametric decay instabilities was supported by the Russian Science Foundation grant 16-12-10043; the calculation of nonlinear matrix elements given in the Appendix is supported by a government contract with the Ioffe Institute, 0040-2014-0023.

6. Appendix

We derive an expression for nonlinear susceptibility that describes the two-plasmon decay of an extraordinary polarization pump wave accompanied by the excitation of two electrostatic (longitudinal) waves. For this, we consider the Vlasov equation for a weakly nonequilibrium electron distribution function in a collisionless magnetized plasma,

$$\left[\frac{\partial}{\partial t} + v_i \frac{\partial}{\partial x_i} - \frac{|e|}{m_e}\left(E_i + \frac{e_{ijk} v_j}{c} H_k\right)\frac{\partial}{\partial v_i} - \omega_c e_{ijz} v_j \frac{\partial}{\partial v_i}\right] f_e = 0\,, \tag{A.1}$$

where e_{ijk} is the totally antisymmetric tensor, $\omega_c = |\omega_{ce}|$, $\mathbf{H} = (0, 0, H)$ is the external magnetic field directed along the z axis, and $\mathbf{E} = \sum_{i=0-2} \mathbf{E}_i$ is the superposition of electric fields, including the electric field of the pump wave that propagates perpendicularly to the external magnetic field,

$$\mathbf{E}_0 = -\mathbf{e}_x \frac{\partial}{\partial x}\phi_0 - \frac{1}{c}\frac{\partial}{\partial t}\mathbf{A}_0 \propto \exp\left(\mathrm{i}k_0 x - \mathrm{i}\omega_0 t\right), \tag{A.2}$$

where the scalar and vector potentials are expressed in terms of the electric field amplitude

$$\phi_0 = \frac{g_0 E_0}{\varepsilon_0 k_0}\,, \qquad \mathbf{A}_0 = -\frac{\mathrm{i}cE_0\mathbf{e}_y}{\omega_0}$$

(g_0 and ε_0 are the transverse components of the dielectric permeability tensor of cold plasma at the frequency ω_0) and the electric field of daughter electrostatic oscillations

$$\begin{aligned} \mathbf{E}_1 &= -\mathbf{e}_x \frac{\partial \phi_1}{\partial x} \propto \exp\left(\mathrm{i}q_1 x + \mathrm{i}\omega_1 t\right), \\ \mathbf{E}_2 &= -\mathbf{e}_x \frac{\partial \phi_2}{\partial x} \propto \exp\left(\mathrm{i}q_2 x - \mathrm{i}\omega_2 t\right), \end{aligned} \tag{A.3}$$

whose frequencies and wavevectors satisfy the decay resonance conditions $\omega_0 = \omega_1 + \omega_2$, $q_2 = q_1 + k_0$. The pump wave polarization vector $\mathbf{e}_0$ defined by the relation $|\mathbf{e}_x|/|\mathbf{e}_y| = \mathrm{i}g_0/\varepsilon_0$ is directed across the external magnetic field. The magnetic field of an extraordinary wave is expressed through the vector potential: $\mathbf{H}_0 = \nabla \times \mathbf{A}_0 = (k_0 c E_0/\omega_0)\mathbf{e}_z$. The solution of Eqn (A.1) is sought using the perturbation theory,

$$f_e = \bar{n} f_M + \sum_{\substack{i=0-2 \\ k=1,2,\ldots}} f_i^{(k)}(\mathbf{v}, \mathbf{r}, t)\,, \tag{A.4}$$

where $\bar{n}$ is the equilibrium density, f_{M} is the Maxwell distribution function normalized to unity,

$$\int f_{\mathrm{M}}(v_\perp, v_z)\,\mathrm{d}^3 v = 1\,,$$

and $f_i^{(1)}$ and $f_i^{(2)}$ are corrections to the equilibrium distribution function of the first and second order in the interacting wave amplitude $i = 0-2$. Substituting (A.4) in Eqn (A.1) and isolating the first- and second-order terms, we first obtain the equation for the linear correction to the distribution function at the frequency of the pump wave and the first UH wave

$$\left(-\mathrm{i}\alpha_s + \mathrm{i}\lambda_s \cos\theta + \frac{\partial}{\partial\theta}\right) f_s^{(1)} = \frac{\bar{n}|e|}{m_{\mathrm{e}}\omega_{\mathrm{c}}}\left(\mathbf{E}_s + \frac{\mathbf{v}\times\mathbf{H}_s}{c}\right)\frac{\partial f_{\mathrm{M}}}{\partial\mathbf{v}}\,,$$

where $s = 0, 1$, $\alpha_0 = \omega_0/\omega_{\mathrm{c}}$, $\alpha_1 = -\omega_1/\omega_{\mathrm{c}}$, $\lambda_0 = k_0 v_\perp/\omega_{\mathrm{c}}$, and $\lambda_1 = q_1 v_\perp/\omega_{\mathrm{c}}$. The solution of the last equation can be found using the Green's function of this equation

$$G_s(\theta,\tau)\big[A(\tau)\big] = \exp\left(\mathrm{i}\alpha_s\theta - \mathrm{i}\lambda_s\sin\theta\right) \times \int_{-\infty}^{\theta} \mathrm{d}\tau \exp\left(\mathrm{i}\lambda_s\sin\tau - \mathrm{i}\alpha_s\tau\right)A(\tau)\,, \quad s = 0, 1\,, \tag{A.5}$$

in the form

$$\begin{aligned} f_0^{(1)} &= -\frac{2|e|f_0 v_\perp E_0}{m_{\mathrm{e}}\omega_{\mathrm{c}} v_{\mathrm{te}}^2}\, G_0(\theta,\tau)\left(\sin\tau - \mathrm{i}\,\frac{g_0}{\varepsilon_0}\cos\tau\right) \\ &= \frac{2\bar{n}|e|v_\perp f_{\mathrm{M}} E_0}{m_{\mathrm{e}}\omega_{\mathrm{c}} v_{\mathrm{te}}^2}\sum_{n=-\infty}^{\infty}\frac{\exp\left(\mathrm{i}n\theta - \mathrm{i}\lambda_0\sin\theta\right)}{n-\alpha_0} \\ &\quad\times\left(\frac{g_0}{\varepsilon_0}\,\frac{nJ_n(\lambda_0)}{\lambda_0} + J_n'(\lambda_0)\right), \\ f_1^{(1)} &= -\frac{2|e|f_0 v_\perp E_1}{m_{\mathrm{e}}\omega_{\mathrm{c}} v_{\mathrm{te}}^2}\, G_1(\theta,\tau)\cos\tau \\ &= \mathrm{i}\,\frac{2\bar{n}|e|}{m_{\mathrm{e}}\omega_{\mathrm{c}} v_{\mathrm{te}}^2} v_\perp f_{\mathrm{M}} E_1 \sum_{m=-\infty}^{\infty}\frac{\exp\left(\mathrm{i}m\theta - \mathrm{i}\lambda_1\sin\theta\right) mJ_m(\lambda_1)}{\lambda_1(m-\alpha_1)}\,. \end{aligned} \tag{A.6}$$

The nonlinear (quadratic) correction to the quasiequilibrium distribution function at the frequency of the second electrostatic wave is a solution of the equation

$$\left(-\mathrm{i}\omega_2 + \mathrm{i}qv_\perp\cos\theta + \omega_{\mathrm{c}}\frac{\partial}{\partial\theta}\right) f_2^{(2)} = \frac{|e|}{m_{\mathrm{e}}}\left\{E_1\frac{\partial f_0^{(1)}}{\partial v_x} + E_0\left[\left(1 - \frac{k_0 v_x}{\omega_0}\right)\mathbf{e}_y + \left(\frac{k_0 v_y}{\omega_0} - \mathrm{i}\,\frac{g_0}{\varepsilon_0}\right)\mathbf{e}_x\right]\frac{\partial f_1^{(1)}}{\partial\mathbf{v}}\right\}.$$

We solve it using Green's function (A.5) as

$$f_2^{(2)} = \frac{|e|}{m_{\mathrm{e}}\omega_{\mathrm{c}}}\, G_2(\theta,\tau)\left[E_1\,\frac{\partial f_0^{(1)}(\tau)}{\partial v_x(\tau)} + \ldots\right].$$

We integrate the derived expression over velocities and multiply it by the electron charge $-|e|$ to obtain the nonlinear charge density at the frequency of the second daughter wave

$$\rho_2^{(2)} = -\frac{|e|^2}{m_{\mathrm{e}}\omega_{\mathrm{c}}}\int_0^{\infty} v_\perp\,\mathrm{d}v_\perp \int_{-\infty}^{\infty}\mathrm{d}v_z \times \int_0^{2\pi}\mathrm{d}\theta\exp\left(\mathrm{i}\alpha_2\theta - \mathrm{i}\lambda_2\sin\theta\right)\int_{-\infty}^{\theta}\mathrm{d}\tau\exp\left(-\mathrm{i}\alpha_2\tau\right)F(\tau)\,, \tag{A.7}$$

where $\alpha_2 = \omega_2/\omega_{\mathrm{c}}$, $\lambda_2 = q_2 v_\perp/\omega_{\mathrm{c}}$, and the function

$$F(\tau) = \exp\left(\mathrm{i}\lambda_2\sin\tau\right)\left\{E_1\frac{\partial}{\partial v_x}f_0^{(1)} + E_0\left[\left(1 - \frac{k_0 v_x}{\omega_0}\right)\mathbf{e}_y + \left(\frac{k_0 v_y}{\omega_0} - \mathrm{i}\,\frac{g_0}{\varepsilon_0}\right)\mathbf{e}_x\right]\frac{\partial f_1^{(1)}}{\partial\mathbf{v}}\right\}$$

must be periodic and expandable into a Fourier series. We substitute linear corrections to distribution function (A.6) in this formula, integrate (A.7) by parts, and then integrate over the angular variables and the longitudinal velocity. The nonlinear susceptibility can be found from the formula

$$\left(\chi_{\mathrm{EM}}^{\mathrm{nl}}|e|\,\frac{A_0}{T_{\mathrm{e}}} + \chi_{\mathrm{L}}^{\mathrm{nl}}|e|\,\frac{\phi_0}{T_{\mathrm{e}}}\right)\varphi_1 = -4\pi\rho_2^{(2)}\,.$$

We use this expression and introduce the notation $J_m' = \partial J_m/\partial\lambda$, where J_m is the Bessel function, to finally obtain

$$\begin{aligned} \chi_{\mathrm{EM}}^{\mathrm{nl}} &= \mathrm{i}q_1 q_2\,\frac{\omega_{\mathrm{pe}}^2}{\omega_{\mathrm{c}}^2}\,\frac{\omega_0}{ck_0}\sum_{p,m}\int_0^{\infty}\mathrm{d}v_\perp\, v_\perp\lambda_0 f_{\mathrm{M}} \\ &\quad\times\left\{\frac{1}{(m-\alpha_1)(p+m-\alpha_2)}\,\frac{mJ_m(\lambda_1)}{\lambda_1}\right. \\ &\quad\times\left[\frac{(p+m)J_{p+m}(\lambda_2)}{\lambda_2}\,\frac{pJ_p(\lambda_0)}{\lambda_0} - J_p(\lambda_0)J_{p+m}(\lambda_2)\right] \\ &\quad+\frac{1}{(p-\alpha_0)(m-\alpha_1)}\,J_p'(\lambda_0)J_{m+p}'(\lambda_2)\,\frac{mJ_m(\lambda_1)}{\lambda_1} \\ &\quad\left.+\frac{m}{(p-\alpha_0)(m-\alpha_2)}\,J_p'(\lambda_0)\,\frac{J_m(\lambda_2)}{\lambda_2}\,J_{m-p}'(\lambda_1)\right\} \\ &\quad+\mathrm{i}q_1 q_2\,\frac{\omega_{\mathrm{pe}}^2}{\omega_{\mathrm{c}}^2}\,\frac{v_{\mathrm{te}}}{c}\sum_{p,m}\int_0^{\infty}\mathrm{d}v_\perp\, v_\perp\,\frac{v_\perp}{v_{\mathrm{te}}}\,\lambda_0 f_{\mathrm{M}} \\ &\quad\times\frac{1}{(m-\alpha_1)(p+m-\alpha_2)}\,\frac{mJ_m(\lambda_1)}{\lambda_1} \\ &\quad\times\left(\frac{pJ_p(\lambda_0)}{\lambda_0}\,J_{p+m}(\lambda_2) - J_p(\lambda_0)\,\frac{(p+m)J_{p+m}(\lambda_2)}{\lambda_2}\right), \end{aligned} \tag{A.8}$$

where $\chi_{\mathrm{EM}}^{\mathrm{nl}}$ is the part of the nonlinear susceptibility that describes the interaction between the electromagnetic component of the pump wave given by the vector potential and daughter electrostatic oscillations;

$$\begin{aligned} \chi_{\mathrm{L}}^{\mathrm{nl}} &= q_1 q_2\,\frac{\omega_{\mathrm{pe}}^2}{\omega_{\mathrm{c}}^2}\sum_{p,m}\int_0^{\infty}\mathrm{d}v_\perp\, v_\perp\lambda_0 f_{\mathrm{M}} \\ &\quad\times\left[\frac{(m+p)p}{(p-\alpha_0)(m+p-\alpha_2)}\,\frac{J_{m+p}(\lambda_2)}{\lambda_2}\,\frac{J_p(\lambda_0)}{\lambda_0}\,J_m'(\lambda_1)\right. \\ &\quad+\frac{(p+m)m}{(m-\alpha_1)(p+m-\alpha_2)}\,\frac{J_{p+m}(\lambda_2)}{\lambda_2}\,J_p'(\lambda_0)\,\frac{J_m(\lambda_1)}{\lambda_1} \\ &\quad\left.+\frac{pm}{(m-\alpha_1)(p-\alpha_0)}\,J_{p+m}'(\lambda_2)\,\frac{pJ_p(\lambda_0)}{\lambda_0}\,\frac{mJ_m(\lambda_1)}{\lambda_1}\right], \end{aligned} \tag{A.9}$$

where $\chi_{\mathrm{L}}^{\mathrm{nl}}$ is the part of the nonlinear susceptibility that describes the interaction between the electrostatic (longitudinal) component of the pump wave given by the potential $\phi_0 = g_0 E_0/(\varepsilon_0 k_0)$ with daughter electrostatic oscillations.

Equations (A.8) and (A.9) are symmetric under permutations of wavevectors and frequencies and satisfy the Manley–Rowe energy relations. Expressions (A.8) and (A.9), which

are equal to zero in the case of the decay of homogeneous oscillations, $k_0 = 0$ [110], allow the complete description of the two-plasmon decay of an extraordinary wave. In addition, $\chi_{\rm L}^{\rm nl}$ enables a description of the decay of short-wave electrostatic vibrations ϕ_0 that result in the excitation of secondary electrostatic vibrations (A.3).

Unfortunately, the integrals over the transverse velocity of electrons in Eqns (A.9) and (A.10) cannot be calculated analytically. We consider the long-wavelength limit of wave oscillation vectors involved in nonlinear interaction, $\lambda_0, \lambda_1, \lambda_2 \ll 1$. This case corresponds to the decay of the pump wave into two daughter UH waves in the vicinity of the upper hybrid resonance. Expanding the Bessel functions in Eqn (A.6) in a series in their arguments, integrating over the transverse velocities, and reducing the terms to a common denominator, we finally obtain the long-wavelength limit of the nonlinear susceptibility. Expressing the extraordinary wave potential and the vector potential in terms of the electric field amplitude for $\omega_2 = -\omega_1 = \omega = \omega_0/2$, we obtain

$$\left(\chi_{\rm EM}^{\rm nl}|e|\,\frac{A_0}{T_{\rm e}} + \chi_{\rm L}^{\rm nl}|e|\,\frac{\phi_0}{T_{\rm e}}\right) = \chi_{\rm e}^{\rm nl}\,\frac{E_0}{H}$$
$$= -\frac{\omega_{\rm pe}^2\omega_{\rm c}^2\omega^2}{(\omega_0^2-\omega_{\rm c}^2)(\omega^2-\omega_{\rm c}^2)^2}\,\frac{q_1q_2k_0c}{\omega_0}\left(7+6\,\frac{g_0}{\varepsilon_0}\,\frac{\omega}{\omega_{\rm c}}-\frac{\omega_{\rm c}^2}{\omega^2}\right)\frac{E_0}{H}\,. \tag{A.10}$$

Formula (A.10) coincides with the formula that can be derived from hydrodynamic equations, thus confirming the validity of Eqns (A.8) and (A.9), which we obtained previously in the integral form.

Because we are considering the case of the decay of an extraordinary pump wave into two UH waves in the vicinity of a UH resonance, we use (A.10) in the analysis of two-plasmon decay.

In analyzing the secondary instability of the primary electrostatic UH wave, which is accompanied by the excitation of electrostatic short-wave IB waves and secondary UH waves, we use the nonlinear susceptibility $\chi_{\rm L}^{\rm nl}$ that follows from Eqn (A.9).

References

1. Piliya A D, in *Proc. of the 10th Intern. Conf. on Phenomena in Ionized Gases, September 13–18, 1971, Oxford, England* (Ed. R N Franklin) (Oxford: Donald Parsons and Co., 1971) p. 320
2. Perkins F W, Flick J *Phys. Fluids* **14** 2012 (1971)
3. Rosenbluth M N *Phys. Rev. Lett.* **29** 565 (1972)
4. Piliya A D *Sov. Phys. JETP* **37** 629 (1973); *Zh. Eksp. Teor. Fiz.* **64** 1237 (1973)
5. Gusakov E Z, Savel'ev A N *Sov. Phys. JETP* **67** 698 (1988); *Zh. Eksp. Teor. Fiz.* **94** (4) 89 (1988)
6. Gusakov E Z, Savel'ev A N *Tech. Phys. Lett.* **19** 226 (1993); *Pis'ma Zh. Tekh. Fiz.* **19** (8) 1 (1993)
7. Zakharov V E, Manakov S V, Novikov S P, Pitaevskii L P *Teoriya Solitonov: Metod Obratnoi Zadachi* (Theory of Solitons: Inverse Problem Method) (Moscow: Nauka, 1980)
8. Piliya A D *JETP Lett.* **17** 266 (1973); *Pis'ma Zh. Eksp. Teor. Fiz.* **17** 374 (1973)
9. Gusakov E Z, Fedorov V I *Sov. J. Plasma Phys.* **5** 263 (1979); *Fiz. Plazmy* **5** 469 (1979)
10. Gusakov E Z, Fedorov V I *Sov. J. Plasma Phys.* **5** 463 (1979); *Fiz. Plazmy* **5** 827 (1979)
11. Gorbunov L M *Sov. Phys. JETP* **40** 689 (1975); *Zh. Eksp. Teor. Fiz.* **67** 780 (1975)
12. Pesme D, Laval G, Pellat R *Phys. Rev. Lett.* **31** 203 (1973)
13. Arkhipenko V I et al. *Sov. J. Plasma Phys.* **13** 398 (1987); *Fiz. Plazmy* **13** 693 (1987)
14. Arkhipenko V I et al. *JETP Lett.* **39** 549 (1984); *Pis'ma Zh. Eksp. Teor. Fiz.* **39** 453 (1984)
15. Arkhipenko V I et al. *Sov. Phys. JETP* **66** 689 (1987); *Zh. Eksp. Teor. Fiz.* **93** 1221 (1987)
16. Arkhipenko V I et al. *JETP Lett.* **53** 247 (1991); *Pis'ma Zh. Eksp. Teor. Fiz.* **53** 233 (1991)
17. Arkhipenko V I et al. *Plasma Phys. Control. Fusion* **40** 215 (1998)
18. Arkhipenko V I et al. *JETP Lett.* **46** 18 (1987); *Pis'ma Zh. Eksp. Teor. Fiz.* **46** 17 (1987)
19. Andreev N E et al. *JETP Lett.* **18** 366 (1973); *Pis'ma Zh. Eksp. Teor. Fiz.* **18** 624 (1973)
20. Silin V P, Starodub A N *Sov. Phys. JETP* **39** 172 (1973); *Zh. Eksp. Teor. Fiz.* **66** 176 (1973)
21. Liu C S, Rosenbluth M N *Phys. Fluids* **19** 967 (1976)
22. Gusakov E Z, Piliya A D, Fedorov V I *Sov. J. Plasma Phys.* **3** 739 (1977); *Fiz. Plazmy* **3** 1328 (1977)
23. Zozulya A A, Silin V P, Tikhonchuk V T *JETP Lett.* **36** 138 (1982); *Pis'ma Zh. Eksp. Teor. Fiz.* **36** 111 (1982)
24. Silin V P, Tikhonchuk V T, Chegotov M V *JETP Lett.* **43** 82 (1986); *Pis'ma Zh. Eksp. Teor. Fiz.* **43** 62 (1986)
25. White R B, Liu C S, Rosenbluth M N *Phys. Rev. Lett.* **31** 520 (1973)
26. Davydova T A *Fiz. Plazmy* **8** 850 (1982)
27. Silin V P, Starodub A N *JETP Lett.* **23** 559 (1976); *Pis'ma Zh. Eksp. Teor. Fiz.* **23** 609 (1976)
28. Zozulya A A, Silin V P, Tikhonchuk V T *JETP Lett.* **38** 52 (1983); *Pis'ma Zh. Eksp. Teor. Fiz.* **38** 48 (1983)
29. Zozulya A A, Silin V P, Tikhonchuk V T *Phys. Lett. A* **99** 224 (1983)
30. Zozulya A A, Silin V P, Tikhonchuk V T *Fiz. Plazmy* **12** 586 (1986)
31. Gusakov E Z, Piliya A D *Sov. J. Plasma Phys.* **6** 277 (1980); *Fiz. Plazmy* **6** 509 (1980)
32. Gusakov E Z, Piliya A D *Fiz. Plazmy* **7** 1328 (1981)
33. Garban-Labaune C et al. *J. Physique Lett.* **41** 463 (1980)
34. Estabrook K, Kruer W L, Lasinski B F *Phys. Rev. Lett.* **45** 1399 (1980)
35. Kruer W L, Valeo E J *Phys. Fluids* **16** 675 (1973)
36. Porkolab M *Phys. Fluids* **17** 1432 (1974)
37. Porkolab M *Phys. Fluids* **20** 2058 (1977)
38. Berger R L, Perkins F W *Phys. Fluids* **19** 406 (1976)
39. Reiman A *Rev. Mod. Phys.* **51** 311 (1979)
40. Bers A, in *Basic Plasma Physics* (Handbook of Plasma Physics, Vol. 2, Eds A A Galeev, R N Sudan) (Amsterdam: North-Holland, 1985); Ttanslated from Russian: in *Osnovy Fiziki Plazmy* Vol. 2 (Moscow: Energoatomizdat, 1984)
41. Wong K L, Wilson J R, Porkolab M *Phys. Fluids* **23** 96 (1980)
42. Bonoli P T, Porkolab M, Englade R *AIP Conf. Proc.* **129** 139 (1985)
43. Golant V E et al. *Sov. Phys. Tech. Phys.* **16** 1980 (1972); *Zh. Tekh. Fiz.* **41** 2492 (1971)
44. Alikaev V V et al. *JETP Lett.* **15** 27 (1972); *Pis'ma Zh. Eksp. Teor. Fiz.* **15** 41 (1972)
45. Golant V E et al., in *Proc. of the 3rd Intern. Symp. on Toroidal Plasma Confinement Garching, 1973* (Garching: Max-Planck-Institut für Plasmaphysik, 1973) paper E5
46. Alikaev V V et al. *JETP Lett.* **35** 140 (1982); *Pis'ma Zh. Eksp. Teor. Fiz.* **35** 115 (1982)
47. Alikaev V V et al. *Fiz. Plazmy* **9** 336 (1983)
48. Alikaev V V et al., in *Proc. of the 11th Europ. Conf. on Controlled Fusion and Plasma Physics, Aachen, 1983*
49. Alikaev V V et al. *Fiz. Plazmy* **13** 3 (1987)
50. Hugill J et al., in *Proc. of the 14th European Conf. on Controlled Fusion and Plasma Physics, Madrid, Spain, 22–26 June 1987* Vol. 11D (Eds F Engelmann, J L Alvarez Rivas) Pt. 3 (Madrid: European Physical Society, 1987) p. 813
51. Lohr J et al., in *IAEA Technical Commitee Meeting on RF Heating and Current Drive, Moscow, 1987*
52. Robinson D C et al., in *Proc. of the 14th European Conf. on Controlled Fusion and Plasma Physics, Madrid, Spain, 22–26 June 1987* Vol. 11D (Eds F Engelmann, J L Alvarez Rivas) Pt. 3 (Madrid: European Physical Society, 1987) p. 814
53. Leuterer F et al. *Nucl. Fusion* **43** 1329 (2003)
54. Burrell K H for the DIII-D Team *Nucl. Fusion* **43** 1555 (2003)
55. Maaßberg H et al. *Plasma Phys. Control. Fusion* **47** 1137 (2005)
56. Giruzzi G et al. *Nucl. Fusion* **51** 063033 (2011)
57. Igami H et al. *EPJ Web Conf.* **87** 02011 (2015)

58. Andreev V F et al. *Plasma Phys. Control. Fusion* **58** 055008 (2016)
59. Höfel U et al., in *Proc. of the 43rd EPS Conf. on Plasma Physics ECA, 4–8 July 2016, Leuven, Belgium* (Europhysics Conf. Abstracts, Vol. 40A) (Mulhouse: European Physical Society, 2016) P4.008
60. Porkolab M, Cohen B I *Nucl. Fusion* **28** 239 (1988)
61. Cohen B I et al. *Rev. Mod. Phys.* **63** 949 (1991)
62. Litvak A G et al. *Phys. Fluids B* **5** 4347 (1993)
63. McDermott F S et al. *Phys. Fluids* **25** 1488 (1982)
64. Bulyginskii D G et al. *Sov. J. Plasma Phys.* **12** 884 (1986); *Fiz. Plazmy* **12** 138 (1986)
65. Laqua H P et al. *Phys. Rev. Lett.* **78** 3467 (1997)
66. Gusakov E Z, Surkov A V *Plasma Phys. Control. Fusion* **49** 631 (2007)
67. Westerhof E et al. *Phys. Rev. Lett.* **103** 125001 (2009)
68. Kubo S et al. *Rev. Sci. Instrum.* **81** 10D535 (2010)
69. Furtula V et al. *Rev. Sci. Instrum.* **83** 013507 (2012)
70. Nielsen S K et al. *Plasma Phys. Control. Fusion* **55** 115003 (2013)
71. Batanov G M et al. *Plasma Phys. Rep.* **39** 444 (2013); *Fiz. Plazmy* **39** 511 (2013)
72. Bruschi A et al. *Nucl. Fusion* **57** 076004 (2017)
73. Karpushov A N et al., in *Proc. of the 33rd European Physical Society Conf. on Plasma Physics, Roma, June 19–23, 2006* (Europhysics Conf. Abstracts, Vol. 30I, Eds F De Marco, G Vlad) (Mulhouse: European Physical Society, 2006) P-1.152
74. Rapisarda D et al. *Plasma Phys. Control. Fusion* **49** 309 (2007)
75. Zurro B et al. *Nucl. Fusion* **53** 083017 (2013)
76. Martínez M et al. *Plasma Phys. Control. Fusion* **60** 025024 (2018)
77. Donné A J H et al. *Phys. Rev. Lett.* **94** 085001 (2005)
78. Kantor M Yu et al. and TEXTOR Team *Plasma Phys. Control. Fusion* **51** 055002 (2009)
79. Vermare L et al. *Plasma Phys. Control. Fusion* **47** 1895 (2005)
80. Kornev V A et al. *Plasma Phys. Rep.* **31** 803 (2005); *Fiz. Plazmy* **31** 867 (2005)
81. Gusakov E Z, Popov A Yu *Phys. Rev. Lett.* **105** 115003 (2010)
82. Gusakov E Z, Popov A Yu *JETP Lett.* **91** 655 (2010); *Pis'ma Zh. Eksp. Teor. Fiz.* **91** 724 (2010)
83. Gusakov E Z, Popov A Yu *Nucl. Fusion* **51** 073028 (2011)
84. Gusakov E Z, Popov A Yu *JETP Lett.* **94** 277 (2011); *Pis'ma Zh. Eksp. Teor. Fiz.* **94** 301 (2011)
85. Gusakov E Z, Popov A Yu *Europhys. Lett.* **99** 15001 (2012)
86. Popov A Yu, Gusakov E Z, Saveliev A N *JETP Lett.* **96** 164 (2012); *Pis'ma Zh. Eksp. Teor. Fiz.* **96** 178 (2012)
87. Gusakov E Z, Popov A Yu, Saveliev A N *Plasma Phys. Control. Fusion* **56** 015010 (2014)
88. Popov A Yu, Gusakov E Z *JETP* **120** 147 (2015); *Zh. Eksp. Teor. Fiz.* **147** 165 (2015)
89. Popov A Yu, Gusakov E Z *Plasma Phys. Control. Fusion* **57** 025022 (2015)
90. Popov A Yu, Gusakov E Z *JETP* **121** 362 (2015); *Zh. Eksp. Teor. Fiz.* **148** 415 (2015)
91. Gusakov E Z, Popov A Yu, Irzak M A *JETP* **123** 723 (2016); *Zh. Eksp. Teor. Fiz.* **150** 833 (2016)
92. Gusakov E Z, Popov A Yu *Plasma Phys. Control. Fusion* **59** 025005 (2017)
93. Gusakov E Z, Popov A Yu *Phys. Plasmas* **23** 082503 (2016)
94. Popov A Yu, Gusakov E Z *Europhys. Lett.* **116** 45002 (2016)
95. Popov A Yu, Gusakov E Z *JETP Lett.* **105** 78 (2017); *Pis'ma Zh. Eksp. Teor. Fiz.* **105** 64 (2017)
96. Gusakov E Z et al. *Plasma Phys. Control. Fusion* **59** 075002 (2017)
97. Gusakov E Z, Popov A Yu *Phys. Plasmas* **25** 012101 (2018)
98. Gusakov E Z, Popov A Yu *JETP* **125** 702 (2017); *Zh. Eksp. Teor. Fiz.* **152** 826 (2017)
99. Gusakov E Z, Popov A Yu *Plasma Phys. Control. Fusion* **60** 025001 (2018)
100. Gusakov E Z, Popov A Yu, Saveliev A N *Phys. Plasmas* **25** 062106 (2018)
101. Gusakov E Z, Popov A Yu, Saveliev A N *Phys. Plasmas* **25** 082117 (2018)
102. Gusakov E Z, Popov A Yu *Nucl. Fusion* **58** 096033 (2018)
103. Akhiezer A I et al. *Elektrodinamika Plazmy* (Electrodynamics of Plasma) (Moscow: Nauka, 1974)
104. Kroll N M *J. Appl. Phys.* **36** 34 (1965)
105. Kovalev V F et al., Preprint No. 177 (Moscow: Lebedev Physical Institute, 1975)
106. Kovalev V F et al. *Pis'ma Zh. Tekh. Fiz.* **1** 1009 (1975)
107. Vysloukh V A, Petnikova V M, Shuvalov V V *Quantum Electron.* **28** 1034 (1998); *Kvantovaya Elektron.* **25** 1062 (1998)
108. Petnikova V M, Shuvalov V V *Quantum Electron.* **38** 1135 (2008); *Kvantovaya Elektron.* **38** 1135 (2008)
109. Piliya A D, Popov A Yu *Plasma Phys. Control. Fusion* **44** 467 (2002)
110. Silin V P *Parametricheskoe Vozdeistvie Izlucheniya Bol'shoi Moshchnosti na Plazmu* (Parametric Effect of High-Power Radiation on Plasma) (Moscow: Nauka, 1973)
111. Andreev V F et al. *Plasma Phys. Control. Fusion* **46** 319 (2003)
112. Vasilkov D G et al., in *Proc. of the 41st EPS Conf. on Plasma Physics, 23–27 June 2014, Berlin, Germany* (Europhysics Conf. Abstracts, Vol. 38F, Eds S Ratynska et al.) (Mulhouse: European Physical Society, 2014) P4.053
113. Tamura N et al. and LHD Experiment Group, in *Proc. of the 3rd EFDA Transport Topical Group Meeting, Córdoba, Spain, September 7–10, 2010* (Garching: EFDA, 2010) O5-03
114. Kubo S et al. *EPJ Web Conf.* **32** 02007 (2012)
115. Eguilior S et al. and TJ-II Team *Plasma Phys. Control. Fusion* **45** 105 (2003)
116. Castejon F et al., in *Proc. of the 36th European Physical Society Conf. on Plasma Physics, Sofia, Bulgaria, June 29 – July 3, 2009* (Europhysics Conf. Abstracts, Vol. 33E, Eds M Mateev, E Benova) (Mulhouse: European Physical Society, 2009) P-4.178
117. van Milligen B Ph et al. and TJ-II Team *Phys. Plasmas* **25** 062503 (2018)